European Journal of Chemistry

View Journal Online
View Article Online

4-Carboxyanilinium dihydrogen phosphate monohydrate, an organophosphate adducts of 4-amino benzoic acid: Structural, vibrational, thermal, and computational studies

Lata Panicker *

Protein Crystallography Section, Bioscience Group, Bhabha Atomic Research Center, Trombay, Mumbai 400085, India

** Corresponding author at: Protein Crystallography Section, Bioscience Group, Bhabha Atomic Research Center, Trombay, Mumbai 400085, India.*
e-mail: lata@barc.gov.in (L. Panicker).

RESEARCH ARTICLE

10.5155/eurjchem.15.1.1-16.2484

Received: 22 October 2023
Received in revised form: 10 December 2023
Accepted: 26 December 2023
Published online: 31 March 2024
Printed: 31 March 2024

KEYWORDS

DSC
FTIR
DFT
X-ray diffraction
Single crystal structure
4-Carboxyanilinium dihydrogen phosphate monohydrate

ABSTRACT

4-Carboxyanilinium dihydrogen phosphate monohydrate (4-$CAH_2PO_4{\cdot}H_2O$), an organophosphate adduct, was synthesized and characterized by single-crystal X-ray diffraction, Fourier transform infrared (FTIR), Differential scanning calorimetry (DSC) and computational analysis performed using CrystalExplorer 21, Gaussian 09W and Multiwfn 3.7 software. The complex 4-$CAH_2PO_4{\cdot}H_2O$ crystallized in the triclinic space group, *P*-1, with two molecules each of 4-carboxyanilinium (4-CA) cations, $H_2PO_4^-$ anions, and water, respectively, in an asymmetric unit. Crystal data for $C_7H_{12}NO_7P$: triclinic, space group *P*-1, a = 8.5238(2) Å, b = 8.9068(2) Å, c = 14.4976(4) Å, α = 106.456(2)°, β = 90.195(2)°, γ = 92.811(2)°, V = 1054.13(5) Å^3, Z = 4, T = 293 K, μ(Cu Kα) = 2.587 mm^{-1}, $Dcalc$ = 1.595 g/cm^3, 18182 reflections measured (6.358° ≤ 2Θ ≤ 146.396°), 4149 unique (R_{int} = 0.1018, R_{sigma} = 0.0521) which were used in all calculations. The final R_1 was 0.0584 (I > 2σ(I)) and wR_2 was 0.1712 (all data). The organic layer containing 4-CA cations and the inorganic layer containing phosphate anions and water molecules in 4-$CAH_2PO_4{\cdot}H_2O$ crystals are connected through a three-dimensional network of strong charge-assisted N–H···O and C-OH···O hydrogen bonds. The fingerprint plot of 4-$CAH_2PO_4{\cdot}H_2O$ obtained indicated that the most prominent interaction corresponds to the short O···H contact, followed by the H···H and H···C contacts. The intermolecular interaction topology of 4-$CAH_2PO_4{\cdot}H_2O$ has been quantitatively analyzed. The 4-$CAH_2PO_4{\cdot}H_2O$ complex was optimized by density functional theory (DFT) with B3LYP/6-31G basis set and the theoretical IR vibrational spectra determined. The noncovalent interaction (NCI) and quantum theory of the atom in the molecule (QTAIM) analysis were done using Multiwfn 3.7 software. 4-$CAH_2PO_4{\cdot}H_2O$ complex structure and its computational analysis are also compared with that of 4-carboxyanilinium dihydrogen phosphate (4-CAH_2PO_4).

Cite this: *Eur. J. Chem.* **2024**, *15(1)*, 1-16 **Journal website**: www.eurjchem.com

1. Introduction

The organic-inorganic hybrid compounds due to their interesting properties and potential applications such as electric, magnetic, non-linear optical, ferroelectric, and catalytic properties have attracted the scientific community [1-3]. The organic-inorganic hybrid compounds have the combined properties of organic and inorganic compounds within one single compound, giving rise to interesting crystal structures and properties. The different components of these hybrid crystals are held together by a strong hydrogen bond, van der Waals interaction, and most likely electrostatic interactions. The synthesis of cocrystals of important pharmaceutical compounds has led to a significant improvement in its solubility and bioavailability [4,5]. Phosphate being biocompatible, ionic cocrystals of organophosphates have been used in drug products. Dihydrogen phosphate salt was found to exhibit superior stability compared to its free base [6].

Benali-Cherif *et al.* [7,8] has reported the crystal structure of *p*-carboxyphenylammonium dihydrogenmonophosphate monohydrate and 4-carboxyanilinium dihydrogen phosphate, respectively. 4-Carboxyanilinium dihydrogen phosphate (4-CAH_2PO_4) crystalizes in space group monoclinic, $P2_1/n$, Z = 4 and the asymmetric unit contains one 4-carboxyanilinium cation and one dihydrogen phosphate anion [8]. In the crystal structure, each *p*-carboxyanilinium cation is connected to five dihydrogen monophosphate anions via hydrogen bonds. As expected, the O atoms of $H_2PO_4^-$ act as proton acceptors or as proton donors, giving rise to a three-dimensional network. The H_2PO_4 tetrahedra are linked together in pairs by strong O-H···O hydrogen bonds. Thus, the three-dimensional hydrogen bonding framework stabilizes the crystal structure of 4-CAH_2PO_4.

The synthesis, characterization, and computational analysis of the 4-carboxyanilinium dihydrogen phosphate monohydrate (4-$CAH_2PO_4{\cdot}H_2O$) as an organophosphate adduct is presented in this article. The single crystal structure, thermal parameters, and vibrational frequency of 4-$CAH_2PO_4{\cdot}2H_2O$ were determined using single crystal X-ray diffraction, DSC, and FTIR spectroscopy, respectively, and the results are reported.

https://dx.doi.org/10.5155/eurjchem.15.1.1-16.2484

Table 1. Crystal data and structure refinement parameters for 4-$CAH_2PO_4{\cdot}H_2O$ at 293 K.

Empirical formula	$C_7H_{12}NO_7P$
Formula weight (g/mol)	253.15
Temperature (K)	293
Crystal system	Triclinic
Space group	*P*-1
a, (Å)	8.5238(2)
b, (Å)	8.9068(2)
c, (Å)	14.4976(4)
α (°)	106.456(2)
β (°)	90.195(2)
γ (°)	92.811(2)
Volume (Å^3)	1054.13(5)
Z	4
ρ_{calc} (g/cm^3)	1.595
μ (mm^{-1})	2.587
F(000)	528.0
Crystal size (mm^3)	0.6 × 0.4 × 0.2
Radiation	Cu Kα (λ = 1.54184)
2Θ range for data collection (°)	6.358 to 146.396
Index ranges	$-10 \le h \le 10$, $-11 \le k \le 10$, $-17 \le l \le 17$
Reflections collected	18182
Independent reflections	4149 [R_{int} = 0.1018, R_{sigma} = 0.0521]
Data/restraints/parameters	4149/0/304
Goodness-of-fit on F^2	1.061
Final R indexes [I≥2σ (I)]	R_1 = 0.0584, wR_2 = 0.1647
Final R indexes [all data]	R_1 = 0.0624, wR_2 = 0.1712
Largest diff. peak/hole (e.Å^{-3})	0.66/-0.43

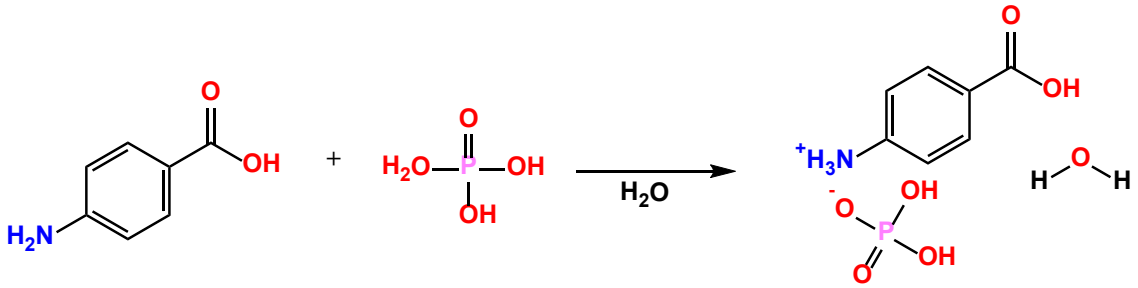

Scheme 1. Synthesis of 4-carboxyanilinium dihydrogen phosphate monohydrate (4-$CAH_2PO_4{\cdot}H_2O$).

Computational analysis obtained using CrystalExplorer 21 is also reported. Density functional theory (DFT) calculation of 4-$CAH_2PO_4{\cdot}H_2O$ in gas phase was carried out with the B3LYP/6-31G basis set. The calculation of noncovalent interaction (NCI) and quantum theory of atom in a molecule (QTAIM) was done using Multiwfn 3.7 software. 4-$CAH_2PO_4{\cdot}H_2O$ complex structure and its computational analysis are also compared with that of 4-carboxyanilinium dihydrogen phosphate (4-CAH_2PO_4).

2. Experimental

2.1. Crystal growth

4-Carboxyanilinium dihydrogen phosphate monohydrate (4-$CAH_2PO_4{\cdot}H_2O$) single crystals were obtained by slow evaporation of the aqueous solution containing, 1:1 molar ratio of 4-amino benzoic acid (4-ABA) and phosphoric acid (H_3PO_4) (Scheme 1). The clear solution obtained by dissolving the ingredient was left undisturbed at 20 °C. Most of the time, first 4-carboxyanilinium dihydrogen phosphate (4-CAH_2PO_4) crystals were obtained [8]. The 4-CAH_2PO_4 crystals were removed by filtering and the remaining solution was left undisturbed. Plate shaped single crystals of 4-$CAH_2PO_4{\cdot}H_2O$ were obtained. Partially deuterated 4-$CAH_2PO_4{\cdot}H_2O$ (*i.e.* *d*4-$CAH_2PO_4.H_2O$) and 4-ABA (*i.e.* *d*4-ABA) wear obtained by re-crystallizing 4-$CAH_2PO_4{\cdot}H_2O$ and 4-ABA, respectively, in D_2O at least three times. In a partially deuterated compound, hydrogen atoms in the $-NH_2$, $-NH_3^+$, $H_2PO_4^-$ and -COOH groups were replaced by deuterium atoms ($-ND_2$, $-ND_3^+$, $D_2PO_4^-$ and -COOD). Almost 100% partial deuteration of 4-$CAH_2PO_4{\cdot}H_2O$ and 4-ABA was achieved, as confirmed by the respective FTIR spectra. Partially deuterated compounds were synthesized for FTIR investigation. FTIR spectra of the deuterated compounds (*d*4-ABA and *d*4-$CAH_2PO_4{\cdot}H_2O$) were useful in assigning functional groups ($-NH_2$ $-NH_3^+$, $H_2PO_4^-$ and -COOH) in 4-$CAH_2PO_4{\cdot}H_2O$.

2.2. Single-crystal X-ray diffraction

Single crystal X-ray diffraction data were collected at ambient temperature (293±2 K) on an Agilent Super Nova diffractometer equipped with a Titan CCD detector using a microfocus X-ray source, CuKα radiation of wavelength 1.54184 Å. Diffraction data were collected at a crystal-to-detector distance of 61 mm with scan width (ω) 1° oscillation per frame. Data collection, indexing, cell refinement, data integration, and reduction were carried out using the CrysAlisPro program [9]. The crystal structure was solved by the direct method using ShelXT [10], completed by difference Fourier syntheses, and refined by full-matrix least squares method using ShelXL [11] accessed by the Olex2 package [12]. The non-H atoms were refined anisotropically. Hydrogen atoms were fixed in their calculated positions. The crystallographic data and refinement details are given in Table 1.

2.3. Differential scanning calorimetry

Mettler Toledo DSC 822 was used for thermal measurements of the samples, with an empty aluminum pan as a reference. Temperature and enthalpy calibration of the instrument was done using cyclohexane and indium. The reported transition temperature, T_c, is the peak temperature.

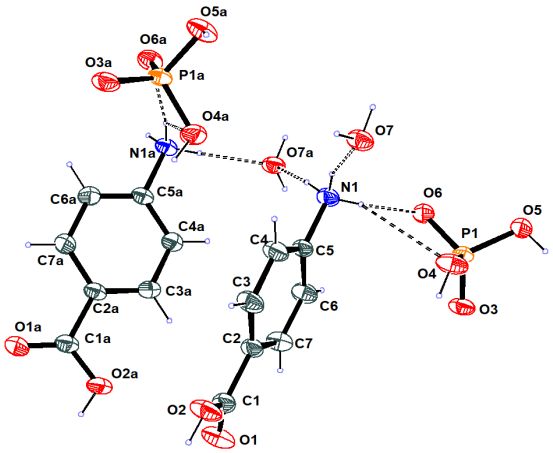

Figure 1. The asymmetric unit of the 4-carboxyanilinium dihydrogen phosphate monohydrate (4-$CAH_2PO_4{\cdot}H_2O$) complex with the atom labeling scheme and hydrogen bond is shown as a dashed line. Displacement ellipsoids are drawn at 50% probability level and H atoms are shown as small spheres of arbitrary radius.

The transition enthalpy of the endothermic curve was calculated using the Mettler Toledo software. The expected experimental errors in temperature and enthalpy values were ±0.1 °C and ±5%, respectively. For measuring the low temperature transition, 25 to 30 mg of crystalline sample was taken, and for the crystal-to-isotropic melting, 4-5 mg of sample was used. The DSC experiments were repeated three times on the same sample to check the reversibility of the transitions, and fresh samples from different syntheses were also repeated to check the reproducibility of the DSC data.

2.4. Fourier transform IR spectroscopy

IR spectra were recorded in wavenumber regions of 4000 to 650 cm^{-1} using a VERTEX 70 FTIR spectrometer (Bruker Optik GmbH, Germany) equipped with a BioATR cell II (Bruker Optik GmbH, Germany), which contains a multireflection silicon crystal. The DLaTGS detector was used to measure the vibrational bands. The spectral resolution was set to 4 cm^{-1}, and for each spectrum 200 scans were recorded. The surface of the ATR crystal was cleaned with distilled water and isopropyl alcohol before loading the sample. The powder sample was placed on the silicon crystal and sealed with a lid. The temperature of the silicon crystal in the BioATR cell II assembly was controlled using an external water bath, Huber Ministate 125 (Peter Huber, Kaltemaschinenbau, Germany). The sample was equilibrated at 298 K for 10 minutes before recording the spectrum. The sample chamber was flushed with dry air during the experiments. The spectrum of air was used as the background prior to each sample analysis. The FTIR spectra recorded were analyzed using OPUS software.

2.5. Hirshfeld surface analyses

CrystalExplorer 21 software [13-15] was used to analyze and visualize Hirshfeld surfaces (HS) [16] and their relative 2D fingerprint plots [17] using the final CIF file of 4-$CAH_2PO_4{\cdot}H_2O$. The normalized contact distance, d_{norm}, and 2D fingerprint plots were used to quantify, visualize, and decode the intercontact in the crystal packing. The dark-red spots on the d_{norm} surface arise as a result of the short interatomic contacts, while the other intermolecular interactions appear as light-red spots. The regions with blue color on the d_{norm} represent longer intercontacts, while the white color indicates the contacts around the van der Waals radius. HS analysis has become a very useful tool for explaining the nature of intermolecular interactions that affect the packing of molecules in crystals [15]. The parameters used in 2D fingerprint plots represent the distances to the Hirshfeld surface from the nuclei (d_i (inside) and d_e (outside)), with respect to the relative van der Waals radius (vdW). Two-dimensional fingerprint plots provide relevant information about the intermolecular contacts in the crystal. The d_{norm} surface was mapped with the color scale in the range -0.8010 a.u. (red) to 1.0648 a.u. (blue). The 2D fingerprint plots (d_i *vs.* d_e) were displayed using the expanded 0.6-2.6 Å range.

2.6. 3D energy framework analysis

CrystalExplorer 21 software [13,14] was used to calculate, visualize, and analyze the 3D energy framework along with the energies of intermolecular interaction in 4-$CAH_2PO_4{\cdot}H_2O$. The intermolecular interaction energies for the energy framework analysis have been estimated using the quantum level of CE-HF/3-21G theory, as available in CrystalExplorer 21 by generating a cluster of 3×3×3 unit cell around the molecule. The density matrices for the neighboring molecules are generated by applying crystallographic symmetry operations to the density matrix of the central molecule [18,19]. For each component of the interaction energy, the scale parameters have been optimized.

2.7. Computational details for quantum chemical calculations

In order to carry out the theoretical computation analysis, the molecular geometry of 4-$CAH_2PO_4{\cdot}H_2O$ is taken from the crystallographically obtained structural data. Theoretical calculations were performed using the Gaussian 09W software package [20] and GaussView6 molecular visualization program [21]. The calculations were performed using density functional theory (DFT) with a hybrid function B3LYP (Becke's three-parameter hybrid functional using the LYP correlation functional) [22,23] at the 6-31G basis set in the gas phase. The compound, 4-$CAH_2PO_4{\cdot}H_2O$, was first optimized geometrically, and this optimized geometry was used to perform further calculations. The vibrational spectra, chemical reactivity, HOMO and LUMO orbital energies, molecular electrostatic potential, and thermodynamic properties of 4-$CAH_2PO_4.H_2O$ were also calculated using DFT.

2.8. Non-covalent interaction and quantum theory of atom in molecule analysis

The NCI and QTAIM analysis were performed with the DFT/B3LYP/6-31G optimized 4-$CAH_2PO_4{\cdot}H_2O$ complex using Multiwfn 3.7 software [24].

Table 2. Bond lengths and angles for 4-carboxyanilinium dihydrogen phosphate monohydrate.

Atom	Atom	Length (Å)	Atom	Atom	Length (Å)
P1A	O6A	1.5072(13)	C5	C4	1.379(3)
P1A	O5A	1.5703(15)	C5	C6	1.391(3)
P1A	O3A	1.5063(15)	C1	C2	1.489(3)
P1A	O4A	1.5695(15)	C2	C7	1.393(3)
P1	O6	1.5086(13)	C2	C3	1.393(3)
P1	O5	1.5689(15)	C2A	C1A	1.493(3)
P1	O3	1.5066(14)	C2A	C3A	1.382(3)
P1	O4	1.5712(15)	C2A	C7A	1.393(3)
O2	C1	1.305(3)	C5A	C6A	1.383(3)
O1	C1	1.221(3)	C5A	C4A	1.379(3)
O2A	C1A	1.307(2)	C7	C6	1.382(3)
N1	C5	1.456(2)	C4	C3	1.383(3)
O1A	C1A	1.215(3)	C3A	C4A	1.383(3)
N1A	C5A	1.461(2)	C6A	C7A	1.380(3)

Atom	Atom	Atom	Angle (°)	Atom	Atom	Atom	Angle (°)
O6A	P1A	O5A	106.05(8)	C3	C2	C1	121.42(18)
O6A	P1A	O4A	108.27(9)	C3	C2	C7	119.36(18)
O3A	P1A	O6A	114.79(9)	C3A	C2A	C1A	121.89(18)
O3A	P1A	O5A	110.65(9)	C3A	C2A	C7A	119.56(18)
O3A	P1A	O4A	109.95(8)	C7A	C2A	C1A	118.54(18)
O4A	P1A	O5A	106.77(9)	C6A	C5A	N1A	118.78(17)
O6	P1	O5	106.05(8)	C4A	C5A	N1A	119.90(18)
O6	P1	O4	108.04(9)	C4A	C5A	C6A	121.32(19)
O5	P1	O4	106.83(9)	C6	C7	C2	120.81(18)
O3	P1	O6	115.04(9)	C5	C4	C3	119.53(18)
O3	P1	O5	110.21(9)	C7	C6	C5	118.71(18)
O3	P1	O4	110.27(8)	O2A	C1A	C2A	114.17(18)
C4	C5	N1	119.37(17)	O1A	C1A	O2A	124.39(19)
C4	C5	C6	121.33(18)	O1A	C1A	C2A	121.43(18)
C6	C5	N1	119.29(17)	C2A	C3A	C4A	120.32(18)
O2	C1	C2	114.40(17)	C7A	C6A	C5A	118.90(19)
O1	C1	O2	124.58(19)	C4	C3	C2	120.23(18)
O1	C1	C2	121.02(19)	C5A	C4A	C3A	119.34(19)
C7	C2	C1	119.21(17)	C6A	C7A	C2A	120.53(19)

Table 3. Inter-atomic bond distances (Å) and angles (°) in 4-$CAH_2PO_4{\cdot}H_2O$.

D-H···A	d(D-H)	d(H···A)	d(D···A)	<D-H··A	
O4-H4B···O5	0.82	1.80	2.555(3)	152.7	1+*x*, +*y*, +*z*
O4A-H4AA···O5A	0.82	1.78	2.544(3)	154.6	1+*x*, +*y*, +*z*
N1-H1A···O5A	0.89	1.88	2.767(3)	171.6	1-*x*, 3-*y*, -*z*
N1-H1B···O3	0.89	1.89	2.771(3)	168.6	-
N1A-H1AC···O3A	0.89	1.92	2.786(3)	164.2	1-*x*, 3-*y*, -*z*
N1A-H1AD···O5	0.89	1.87	2.754(3)	173.2	1+*x*, +*y*, +*z*

3. Results and discussions

3.1. Single crystal X-ray diffraction

The single crystal structure of 4-carboxyanilinium dihydrogen phosphate monohydrate (4-$CAH_2PO_4{\cdot}H_2O$) was obtained at 293 K. The bond distance and angles of 4-$CAH_2PO_4{\cdot}H_2O$ are given in Table 2. The selected distances and angles of the interatomic bonds of 4-$CAH_2PO_4.H_2O$ are given in Table 3. The ORTEP drawing of the asymmetric unit of 4-$CAH_2PO_4{\cdot}H_2O$ with the numbering scheme and hydrogen bond is given in Figure 1 [25]. In the crystal structure, the transfer of a proton from the inorganic acid results in the protonation of the amino group (NH_2) of 4-ABA and forms the 4-carboxyanilinium cation (with +1 charge). Therefore, the chemical formula of 4-$CAH_2PO_4{\cdot}H_2O$ is $2(NH_3{}^+C_6H_4COOH)$: $2(H_2PO_4{}^-)$:$2H_2O$.

3.1.1. 4-Carboxyanilinium dihydrogen phosphate monohydrate crystal structure and packing at 293 K

4-$CAH_2PO_4{\cdot}H_2O$ crystal structure belongs to the triclinic space group *P*-1, *Z* = 4, with two molecules each of 4-carboxyanilinium cations, dihydrogen phosphate anions ($H_2PO_4{}^-$) and water in an asymmetric unit (Figure 1). The crystal structure view of 4-$CAH_2PO_4{\cdot}H_2O$ along the *a*-axis is shown in Figure 2a. It forms an alternate organic and inorganic layered structure that is parallel to the (100) plane (Figure 2). These layers contain crystallographically independent 4-carboxyanilinium cations (in the organic layer) and dihydrogen phosphate anions ($H_2PO_4{}^-$) and water molecules (in the inorganic layer) which are stabilized by an ionic and three-dimensional network of hydrogen bonds between the 4-carboxyanilinium cations and dihydrogen phosphate anions and water molecule. The phosphorus atom in dihydrogen phosphate ($H_2PO_4{}^-$) anions is tetrahedrally bonded to two oxygen and two OH groups. The lengths of the P-O bonds where the P atom is connected to O are in the range 1.5063(15) Å to 1.5086(15) Å. For P atom bond to OH group, the P-O lengths are in the range 1.5712(15) to 1.5689(14) Å. As expected, the protonated P-O link is significantly longer than that of the unprotonated bonds. The O-P-O bond angles of $H_2PO_4{}^-$ anions are in the range 106.04(8)° to 115.05(9)°. These lengths and angles of the bonds are in good agreement with those observed in similar compounds [7, 8].

In Figure 2a-c, it is observed that the $H_2PO_4{}^-$ anion in the inorganic layer forms a long chain by hydrogen bond interaction between the P-OH and -P=O groups of adjacent $H_2PO_4{}^-$ anions in the same layer (Figure 2b). Each inorganic layer consists of two such chains of P–OH···O=P hydrogen bonds. These P–OH···O hydrogen bonds help stabilize the crystal structure. Therefore, the O atoms of the $H_2PO_4{}^-$ moiety act as proton acceptors or as proton donors, resulting in a three-dimensional network. The alternate anions in these chains have the same orientation. Each $H_2PO_4{}^-$ anion forms a hydrogen bond with two molecules of water, two molecules of -4CA, and two molecules of $H_2PO_4{}^-$ (Figure 2c). The phosphate layers are interconnected by 4-CA ions of the organic layers through strong ionic and hydrogen bond interactions with both the $-NH_3{}^+$ and -COOH groups of two different 4-CA cations.

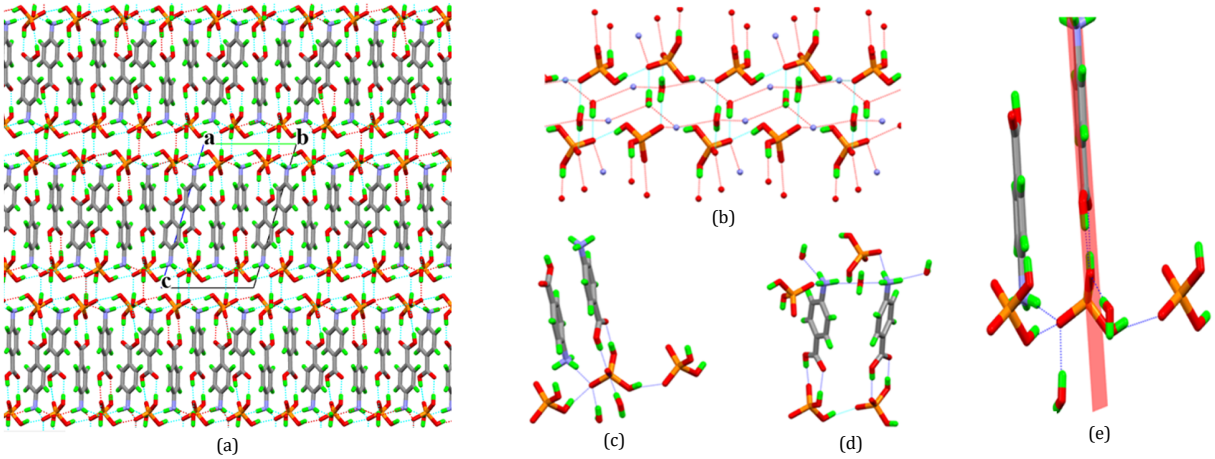

Figure 2. The crystal structure of 4-$CAH_2PO_4{\cdot}H_2O$, (a) view along *a*-axis with 3-D projection of the layer parallel to the (100) plane (b) arrangement of $H_2PO_4^-$ anions in the inorganic layer (c) hydrogen bonding with $H_2PO_4^-$ anion (d) hydrogen bonding with 4-CA and (e) plane drawn using the cyclic acid dimer atoms (formed between the -COOH and -POOH groups).

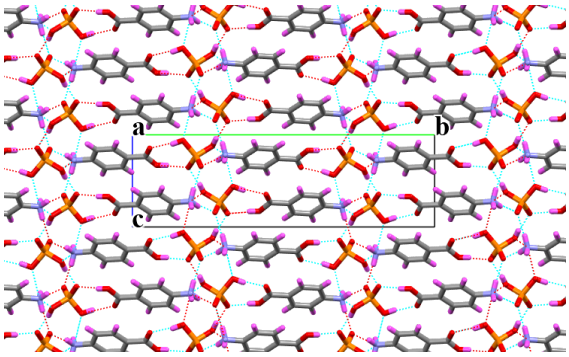

Figure 3. The crystal structure of 4-carboxyanilinium dihydrogen phosphate (4-CAH_2PO_4) (Reference [8] CCDC Deposition Number 647348) viewed along *a*-axis showing 3-D projection of the layer parallel to the (100) plane.

The geometry of the organic cations in 4-$CAH_2PO_4{\cdot}H_2O$ crystals is in good agreement with the structures reported for the 4-carboxyanilinium cations [26,27]. In 4-$CAH_2PO_4{\cdot}H_2O$ crystal structure within the horizontal organic layer, the adjacent 4-carboxyanilinium ions are arranged in head-to-tail orientation (Figure 2a). The -COOH (-C=O and -C-OH) group of the 4-CA cation forms a hydrogen bond with the -P=O and -P-OH groups of the same anion (Figure 2d). This leads to the formation of a cyclic arrangement and all atoms involved in hydrogen bonding lie in the same plane (Figure 2e). The interesting observation is that there is no hydrogen bond interaction between neighboring 4-carboxyanilinium cations. The $-NH_3$ group forms hydrogen bonds with two water molecules and one $H_2PO_4^-$ anion, respectively (Figure 2d). The 4-CA-cations are held in the organic layer by strong H-bonding and ionic interactions with anions and water on both sides. Such an extensive three-dimensional hydrogen-bonding framework stabilizes the crystal structure.

4-Carboxyanilinium dihydrogen phosphate monohydrate (4-$CAH_2PO_4{\cdot}H_2O$) and 4-carboxyanilinium dihydrogen phosphate (4-CAH_2PO_4) (Figure 3) [8] both are organo-phosphate adducts of 4-amino benzoic acid. However, the crystal structure of 4-$CAH_2PO_4{\cdot}H_2O$ is different from that of 4-CAH_2PO_4. In 4-CAH_2PO_4, the inorganic layer has one chain of P-OH···O interlink, while in 4-$CAH_2PO_4{\cdot}H_2O$ there are two such chains within the same layer. In the 4-CAH_2PO_4 crystals, four $H_2PO_4^-$ ions interact *via* a H-bond with the NH_3^+ group of three different 4-carboxyanilinium cations, while in 4-$CAH_2PO_4{\cdot}H_2O$ crystal, the $-NH_3$ group–forms hydrogen bonds with two molecules of water and one O atom of the $H_2PO_4^-$ anion. In both crystal structures, the -COOH group of the 4-CA cation forms a hydrogen bond with the -P=O and -P-OH groups of the same anion. This interaction leads to the formation of a cyclic arrangement of all atoms involved in hydrogen bonding. However, in the case of 4-CAH_2PO_4, these atoms do not lie in the same plane. Thus, the formation of different crystal structures from the same reaction mixture is an important property and characteristic of organic molecules.

3.2. Differential scanning calorimetry

The DSC heating thermograms of 4-$CAH_2PO_4{\cdot}H_2O$ and 4-ABA were obtained in the temperature range of 173 to 293 K and 293 to 480 K, respectively. The thermal parameters, transition temperatures, and transition enthalpies obtained from the DSC curves are given in Table 4. No transition is seen in the low temperature range (173 to 293 K). 4-$CAH_2PO_4{\cdot}H_2O$ when heated gave endothermic transitions at 323.35, 374.16 and 459.42 K, respectively, and the corresponding enthalpy associated with it was -10.80, -12.5 and -276.82 J/g, respectively (Table 4, Figure 4). Thus, the heating thermogram of 4-$CAH_2PO_4{\cdot}H_2O$ obtained was different from that of 4-ABA, indicating formation of a new compound (Figure 4). The transitions seen at 323.35 and 374.16 K, which is irreversible, could be associated with the loss of crystallization water. This is supported by the observation that the clear crystal became opaque when heated to 374 K. Additionally, the sample had undergone weight loss. The broad isotropic melting transition is seen at 459.42 K (Figure 4). In 4-CAH_2PO_4, only a broad isotropic melting transition is seen at 466.33 K (Table 4).

Table 4. Transition temperatures and enthalpies of crystal to isotropic melting in 4-$CAH_2PO_4{\cdot}H_2O$, 4-CAH_2PO_4, and 4-ABA.

Sample	Isotropic melting	
	Peak temperature (K)	Transition enthalpy (J/g)
4-ABA	461.20	-186.80
4-$CAH_2PO_4{\cdot}H_2O$	323.24	-10.80
	374.16	-12.50
	459.42	-276.82
4-CAH_2PO_4	466.33	-253.53

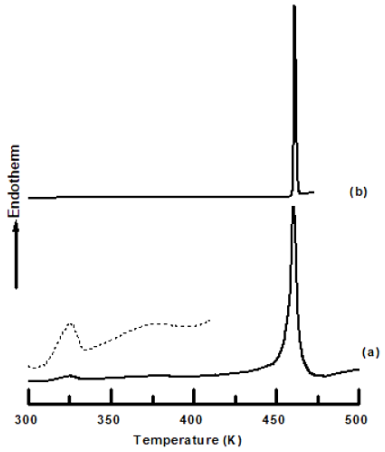

Figure 4. DSC heating thermograms at 5 °C/min of (a) 4-$CAH_2PO_4{\cdot}H_2O$ and (b) 4-ABA in the temperature range of 293 to 480 K. The dotted curve gives the transition seen in 4-$CAH_2PO_4{\cdot}H_2O$ from 300 to 410 K (expanded 16 times).

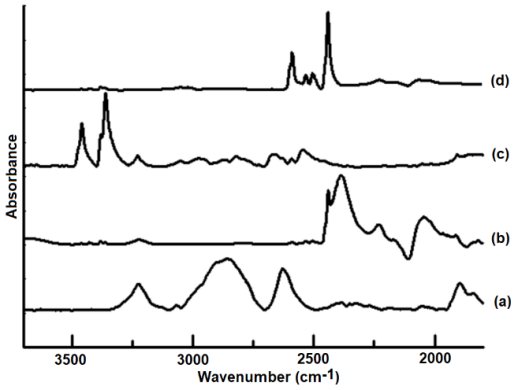

Figure 5. FTIR spectra at 298 K of (a) 4-$CAH_2PO_4{\cdot}H_2O$, (b) *d*4-$CAH_2PO_4.H_2O$, (c) 4-ABA and (d) *d*4-ABA in 3600-1800 cm^{-1}.

3.3. FTIR spectra

FTIR spectra of 4-$CAH_2PO_4{\cdot}H_2O$, *d*4-$CAH_2PO_4{\cdot}H_2O$, 4-ABA and *d*4-ABA at 298 K were recorded in the 1800-3600 cm^{-1} and 650-1800 cm-1 region, and are shown in Figures 5 and 6, respectively. The IR vibrational mode assignments for the different modes observed in these compounds are given in Table 5. The vibrational spectra and assignments of most of the modes of 4-ABA and *d*4-ABA obtained are consistent with the reported data [28-30]. The spectrum of the deuterated compound was analyzed and used for the assignment of functional groups (-NH_2 -NH_3^+, -OH). When comparing the 4-$CAH_2PO_4{\cdot}H_2O$ spectra with those of the parent compound, 4-ABA, it is clearly seen that the various vibrational bands of 4-ABA are affected by the complexation (Figures 5 and 6) (Table 5). This is due to the different types of intermolecular interactions through hydrogen bonds existing in 4-ABA and 4-$CAH_2PO_4{\cdot}H_2O$, respectively. Thus, the mode frequencies of the functional groups that participate in the hydrogen bonding are often altered; the extent of the shift depends on the strength of interaction. Therefore, the FTIR spectrum of 4-$CAH_2PO_4{\cdot}H_2O$, is significantly different from those of the parent component 4-ABA.

3.3.1. The vibrations of 4-carboxyanilinium cations and phosphate anions

The compound 4-$CAH_2PO_4{\cdot}H_2O$ is an ionic molecular crystal with the -NH_3^+, -COOH and $H_2PO_4^-$ groups. However, the 4-ABA molecule is neutral with -NH_2 and -COOH groups. In the 4-ABA crystal structure pair of organic molecules, 4-ABA is linked together to form cyclic -COOH dimers through a strong O-H···O hydrogen bond arranged around a center of symmetry (Figure 7a). The -NH_2 group also forms a hydrogen bond with the -COOH group (Figure 7a). However, in 4-$CAH_2PO_4{\cdot}H_2O$, (a) -NH_3^+ forms hydrogen bond with $H_2PO_4^-$ and water molecules and (b) -COOH forms hydrogen bond with $H_2PO_4^-$ (Figure 7b). The differences in hydrogen bonding interactions observed in these crystals are clearly reflected in the FTIR spectra. The mode assignment of 4-$CAH_2PO_4{\cdot}H_2O$ (*d*4-$CAH_2PO_4{\cdot}H_2O$) crystals was carried out by comparing the observed IR frequencies to those reported for the parent compound 4-ABA (*d*4-ABA) [28-30].

Table 5. Assignment of the IR vibrational frequencies (cm^{-1}) of the bands observed in 4-ABA, *d*4-ABA, 4-$CAH_2PO_4{\cdot}H_2O$ and *d*4-$CAH_2PO_4{\cdot}H_2O$ measured at 298 K and the DFT calculated frequencies of 4-$CAH_2PO_4{\cdot}H_2O$.

4-ABA	*d*4-ABA	4-$CAH_2PO_4{\cdot}H_2O$	*d*4-$CAH_2PO_4{\cdot}H_2O$	Assignments *	4-$CAH_2PO_4{\cdot}H_2O$ (DFT)
3458	-	-	-	$\nu_{as}NH_2$	-
3361	-	-	-	$\nu_{s}NH_2$	-
3090 to 2550	-	3100 to 2500	-	νOH	3725, 3348 (water), 3675, 3655 ($H_2PO_4^-$), 3630 (4-CA)
-	-	3226, 3067 2660, 2628	-	$\nu_{as}NH_3^+$ $\nu_{s}NH_3^+$	3371, 2892, 2568 (4-CA)
-	2590	-	-	$\nu_{as}ND_2$	-
-	2533, 2504, 2441	-	-	$\nu_{s}ND_2$	-
-	2323 to 1867	-	-	ν(O-D)	-
-	-	-	2441, 2387, 2229	$\nu_{as}ND_3^+$, $\nu_{s}ND_3^+$, ν(O-D)	-
-	-	-	2044, 1912	$\nu_{s}ND_3^+$ ν(O-D)	-
-	-	1897	-	-	1796, 1765
1661	1658	1658s	1657s	νC=O	1731
1622	-		-	$\beta_{asym}NH_2$	-
1597	1599	1612m	1603	8a (C-C stretching vibration)	1693
1571	1570	1578	1568w	8b (C-C stretching vibration)	1652
-	-	1557m	-	$\beta_{asym}NH_3^+$	1693, 1652
1520	1521	1512 m	1516w	19a (C-C stretching vibration)	1645
1441	1435	1452 m	1432	19b (C-C stretching vibration)	1570
1419	1420	1426 m	1422	9b (C-H in-plane bending vibration)	1485
1419-1395	-	1419-1395	-	β_{OH}	1390 (-4CA)
-	1364	-	-	$\beta_{asym}ND_2$	-
	-	-	1369	$\beta_{asym}ND_3^+$	-
1311	1312	1321 m	1327w	14 (C-C stretching vibration)	1269
1286	1288	1299 m	1293 m	νC-OH / 14, β_{OD}	1199
		1212	1215	$\delta_s(PO_HH)$, $\delta_{as}(PO_HH)$	1172,1146, 1109
1171	1175	1189 m	1175	9a (C-H in-plane bending vibration)	1186
1128	1125	1132 m	1125m	7a/9a (C-H stretching vibration)	1057, 1085
-	-	1093m, 1019m	1059, 1043s	$\nu_{as}(PO)$, $\nu_{s}(PO)$, $\beta_{sym}NH_3^+$, νC-OD, β_{OH}/γ_{OH}	1109, 1146, 1172
-	-	999 s, 958 s	1015s, 962	$\nu_{as}(PO_H)$, $\nu_{s}(PO_H)$	1012, 1026
1069	-	-	-	$\beta_{sym}NH_2$	-
-	1043, 1061	-	-	νC-OD	-
962w	963w	-	-	17a (C-H out-of-plane vibration)	898
922	-	-	-	γ_{OH}	677
889	888	887	899	5/ νC=O	879
841m	842m	852v	844	17b (C-H out-of-plane vibration)	876
817	817	839m	844	10a (C-H out-of-plane vibration)	862
-	-	-	-	$\beta_{sym}ND_3^+$	-
771	771	760m	772m	1 (radial skeletal vibration)	845
-	746	-	752	γ_{OD}	-
698	700	687, 670	724, 701	4 (γ skeletal vibration), $\rho(PO_2)$	782, 735, 725 (PO)

* ν, stretching; β, in plane; γ, out of plane deformations; ρ, rocking; τ, twisting; δ, scissoring; s, strong; m, medium; w, weak.

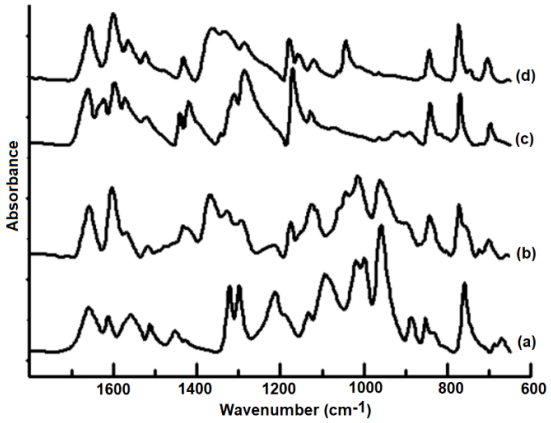

Figure 6. FTIR spectra at 298 K of (a) 4-$CAH_2PO_4.H_2O$, (b) *d*4-$CAH_2PO_4.H_2O$, (c) 4-ABA and (d) *d*4-ABA in 1800-650 cm^{-1}.

The FTIR spectra of 4-$CAH_2PO_4{\cdot}H_2O$ exhibit bands corresponding to the vibration modes of the organic molecule 4-carboxyanilinium (4-CA^+) and the dihydrogen phosphate ($H_2PO_4^-$) group. In 4-$CAH_2PO_4{\cdot}H_2O$, the asymmetrical (ν_{asym}) and symmetrical (ν_{sym}) stretching vibration bands of the N-H bonds (of the $-NH_3^+$ group) are observed as a broad band with multiple peaks in 3226 to 2628 cm^{-1}. The broadened and decreased values of the N-H stretching frequency suggest the presence of a very strong N-H···O hydrogen bond in 4-$CAH_2PO_4{\cdot}H_2O$ than in 4-ABA (Table 5). From the crystallographic data, it is seen that in 4-ABA the $-NH_2$ group forms a weak hydrogen bond with the C=O group, while in 4-$CAH_2PO_4{\cdot}H_2O$ the $-NH_3^+$ group forms a strong hydrogen bond with the P=O groups and water molecules. On deuteration, the N-H stretch bands of 4-ABA and 4-$CAH_2PO_4{\cdot}H_2O$, respectively, shift in the region 2044-2590 cm^{-1}, which corresponds to the N-D stretching band (Table 5). The broad band observed in the region 3100 to 2500 cm^{-1} is assigned to the symmetric stretching vibration bands of the OH bonds.

In 4-$CAH_2PO_4{\cdot}H_2O$ the C=O band is observed at higher frequency suggesting a weak hydrogen bond interaction in 4-$CAH_2PO_4.H_2O$ as compared to that in 4-ABA (Table 5).

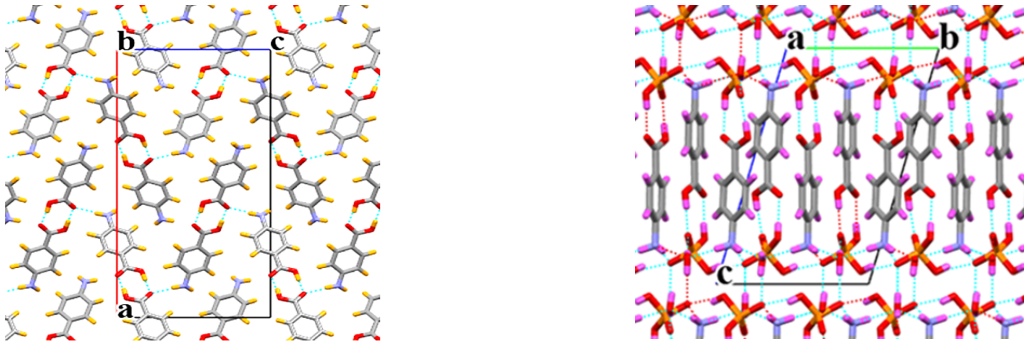

(a) (b)

Figure 7. Unit cell representation of (a) 4-ABA and (b) 4-$CAH_2PO_4{\cdot}H_2O$. Crystallographic data reference numbers AMBNAC09 for 4-ABA and CCDC Deposition Number 2288228 for 4-$CAH_2PO_4{\cdot}H_2O$.

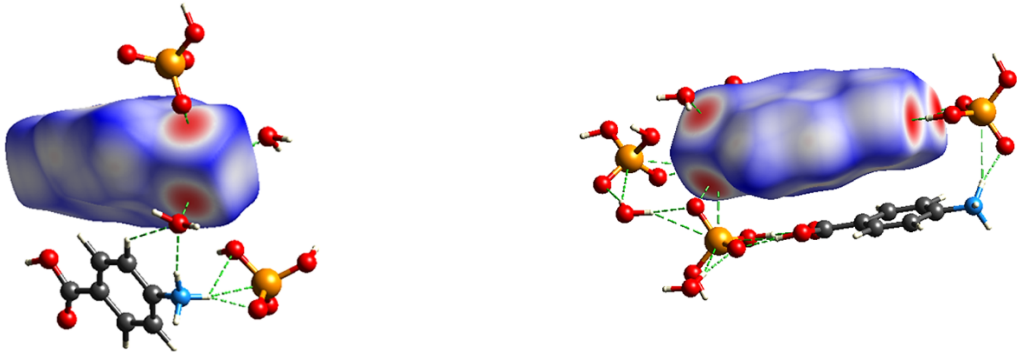

(a) (b)

Figure 8. Three-dimensional view of Hirshfeld surface in 4-$CAH_2PO_4{\cdot}H_2O$ plotted over d_{norm} in the range -0.801 to 1.0648 a.u. using one 4-CA molecule in an asymmetric unit. HS with hydrogen bond interaction within the molecules in (a) an asymmetric unit and (b) in a unit cell.

The bands in 650-1700 cm^{-1}, whose frequencies are not affected by deuteration, are assigned to the ring modes 8a, 8b, 19a, 19b, 9b, 14, 9a, 7a, 12, 17a, 5, 17b, 10a, 1 and 4, respectively, consistent with the earlier work (Table 5) [28-30]. The band at 1557 cm^{-1} in 4-$CAH_2PO_4.H_2O$, which shifts to a lower frequency 1369 cm^{-1} on deuteration, is assigned to $\beta_{asym}NH_3^+$. The band at 1419-1395 cm^{-1} in 4-$CAH_2PO_4{\cdot}H_2O$, is assigned to β_{OH}. In its deuterated counterpart, the β_{OD} is seen at 1293 cm^{-1}. The band observed at 1293 cm^{-1} in 4-$CAH_2PO_4{\cdot}H_2O$, can be assigned to $\nu_{C\text{-}OH}$. On deuteration, the $\nu_{C\text{-}OD}$ band is seen at a lower frequency.

The isolated PO_4^{3-} tetrahedron has Td symmetry [31]. However, in the $H_2PO_4^-$ tetrahedron, the localization of two protons on two oxygen atoms reduces the ideal symmetry from Td to C2v. This gives rise to 15 internal vibrations active in IR and Raman, but exceptional has been the A2 mode, which is only Raman active [32,33]. However, in the crystal, the $H_2PO_4^-$ tetrahedron has a lower local symmetry C1, and therefore anisotropic crystal fields can increase the degeneracy and allow inactive modes to be active. The correlation of group to subgroup shows that these modes in $H_2PO_4^-$ can be divided into (2A1 + B1 + B2) stretching and (2A1 + A2 + B1 + B2) bending vibrations with C2v symmetry. $H_2PO_4^-$ anion interpretation is made in terms of internal modes of two atomic groups, PO_2 (O=P=O) and $P(OH)_2$ (HO-P-OH). According to reference [34], the FTIR spectrum of $H_2PO_4^-$ exhibits five sharp bands at 1156, 1077, 944, 879, and 521 cm^{-1}, which is assigned to (two P-O stretches, two P-O_H stretches, and O-P-O bending modes) $\nu_{as}(PO)$, $\nu_s(PO)$, $\nu_{as}(PO_H)$, $\nu_s(PO_H)$ and $\delta(OPO)$, respectively, These are two stretching vibrations, asymmetric and symmetric of PO_2 group, and those related to $P(OH)_2$. The bending modes of the $H_2PO_4^-$ group are observed at lower frequencies. The broad shoulder at 1213 cm^{-1} is assigned to the two P-O_H-H bending modes bands, $\delta_s(PO_HH)$ and $\delta_{as}(PO_HH)$ [34,35]. The band at 748 cm^{-1} corresponds to the rocking $\rho(PO_2)$ vibrations.

4-$CAH_2PO_4{\cdot}H_2O$ compound consists of a dihydrogen phosphate ion ($(HO)_2PO_2^-$). In the crystal structure, these ions exist as a polymeric chain by forming P=O···H-O-P hydrogen bond between the adjacent $H_2PO_4^-$ ions. The bending vibration of P-OH, $\delta_s(PO_HH)$ and $\delta_{as}(PO_HH)$ occur as abroad band at 1212 cm^{-1}. The vibrational bands observed at 1093 and 1019 cm^{-1} are attributed to the asymmetric ($\nu_{as}(PO)$) and symmetric ($\nu_s(PO)$) stretching vibrations of the P-O bond. The vibrational bands seen at 999 and 958 cm^{-1} are ascribed to the asymmetric ($\nu_{as}(PO_H)$) and symmetric ($\nu_s(PO_H)$) stretching vibrations of the P-O_H bond. The vibration bands, $\nu_{as}(PO)$, $\nu_s(PO)$, $\nu_{as}(PO_H)$ and $\nu_s(PO_H)$ are not affected by deuteration (Table 5). But the vibrational bands, $\delta_s(PO_HH)$ and $\delta_{as}(PO_HH)$ shows shift to lower frequency on deuteration. When compared to IR spectra of neat $H_2PO_4^-$ ions, the $\nu_{as}(PO)$ and $\nu_s(PO)$ vibrational bands in 4-$CAH_2PO_4.H_2O$ show a blue shift (decrease) of 63 and 58 cm^{-1}, respectively, indicating a strong H-bond with P=O in the compound. The $\nu_{as}(PO_H)$ and $\nu_s(PO_H)$ vibrational bands show a red shift (increase) of 55 and 79 cm^{-1}, respectively, indicating a reduced H-bonding interaction with P-OH in the compound than the neat $H_2PO_4^-$ ions. However, the bending vibration of P-OH, $\delta_s(PO_HH)$, and $\delta_{as}(PO_HH)$ is not affected by the complex formation. The vibrational spectra and assignments of the modes of $(HO)_2PO_2^-$ obtained are consistent with those reported for dihydrogen phosphate compounds [32]. Therefore, most of the vibrational mode assignment of 4-$CAH_2PO_4{\cdot}H_2O$ could be done by comparing the IR frequencies of its internal mode region with those observed in the parent compounds 4-ABA and H_3PO_4.

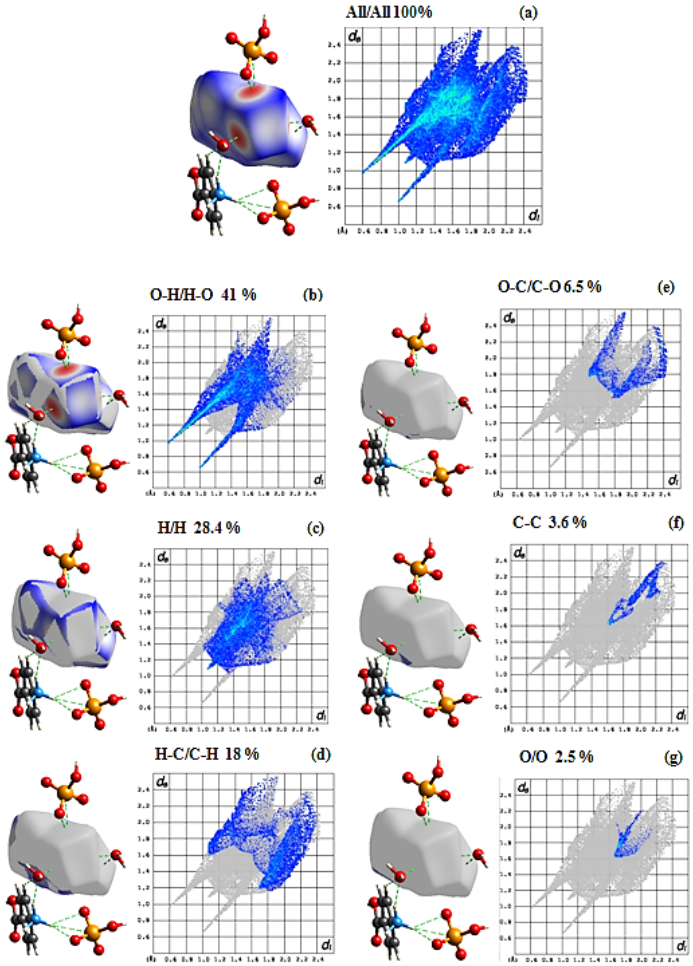

Figure 9. Two-dimensional fingerprint graphs of 4-$CAH_2PO_4{\cdot}H_2O$ showing the contributions of (a) all intermolecular contacts and individual interactions: (b) O···H/H···O, (c) H···H, (d) H···C/C···H (e) O···C/C···O, (f) C···C and (g) O···O. The outline of the full fingerprint plot is shown in grey. HF surfaces highlight the relevant d_{norm} surface patches associated with the specific intermolecular contacts. The percentage contribution is specified for each contact.

3.4. Hirshfeld surface analysis

The intermolecular interactions in 4-$CAH_2PO_4{\cdot}H_2O$ were investigated and visualized by HS analyzes performed using CrystalExplorer 21 [13,19]. One of the 4-CA molecules from the asymmetry unit was used to generate HS. The d_{norm} mapped on the HS shows short intermolecular contacts as red spots corresponding to C-OH···O, C=O···H and N-H··O hydrogen bonds (Figure 8).

The fingerprint plot of 4-$CAH_2PO_4{\cdot}H_2O$ showing all intermolecular contacts and the contribution of the individual O···H/H···O, H···H, H···C/C···H, O···C/C···O and O···O contacts, respectively, are illustrated in Figure 9 together with their relative contributions to the Hirshfeld surface. The most prominent interaction corresponds to the short O···H/H···O contacts; they contribute 41% to the overall surface contact and form a pair of spikes (Figure 9b). They are due to the intermolecular C-H···O/C=O···H hydrogen bond. H···H contacts contributing 28.4% to the overall surface are depicted in Figure 9c. The presence of C-H···π interactions gives rise to a pair of characteristic wings in the fingerprint graph decomposed into H···C/C···H contacts (Figure 9d) contributing 18 % to the HS. The contributions of other contacts O···C/C···O, C··C, and O···O of 6.5, 3.6, and 2.5 %, respectively, to the Hirshfeld surface are negligible. Two-dimensional finger print plots of 4-CAH_2PO_4 (Reference [8] CCDC deposition number 647348) showing contributions of (a) all intermolecular contacts and individual interactions, (b) O···H/H···O (47.7 %), (c) H···H (28.9 %) (d) H···C/C···H (8.6 %) (e) O···C/C···O (8.9 %) and (f) C···C (5.9 %) are shown in Figure 10. When comparing the individual interactions of 4-$CAH_2PO_4{\cdot}H_2O$ with those of 4-CAH_2PO_4 as accepted, both show a similar type of interactions (Figure 11). However, the values were different, indicating the difference in intermolecular interaction (Figure 11).

3.5. Energy framework analysis

The 3D topology of the strong charge-assisted hydrogen bonds in 4-$CAH_2PO_4{\cdot}H_2O$ was obtained by plotting the energy framework. To obtain the 3D topology, the interaction energies obtained are used to construct representative cylinders that connect the molecules, where the thickness of the cylinders is set proportional to the values of the interaction energy. The resulting 3D frameworks or topologies of interactions are termed energy frameworks [14]. Therefore, the energy frameworks allow us to examine 'cooperative effects' in intermolecular interactions across the crystal [13,14]. The energy frameworks allow one to find the electrostatic (red), dispersion (green) and total energy (blue for binding, gold for non-binding) terms separately. The total intermolecular interaction energy (E_{tot}) given is the sum of four energy terms: electrostatic (E_{ele}, red), polarization (E_{pol}), dispersion (E_{disp}, green) and exchange repulsion (E_{rep}) with scale factors of 1.019, 0.651, 0.901 and 0.811, respectively (for CE-HF/3-21G quantum level of theory) [18,19].

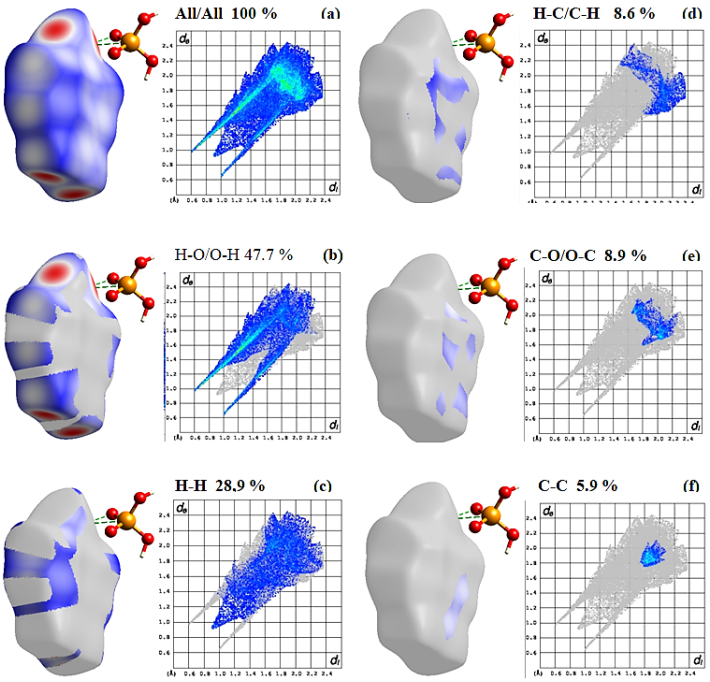

Figure 10. Two-dimensional fingerprint graphs of 4-CAH_2PO_4 (Reference [8] CCDC Deposition Number 647348) showing contributions of (a) all intermolecular contacts and individual interactions: (b) O···H/H···O, (c) H···H, (d) H···C/C···H, (e) O···C/C···O and (f) C···C. The outline of the full fingerprint plot is shown in grey. HF surfaces highlight the relevant d_{norm} surface patches associated with specific intermolecular contacts. The percentage contribution is specified for each contact.

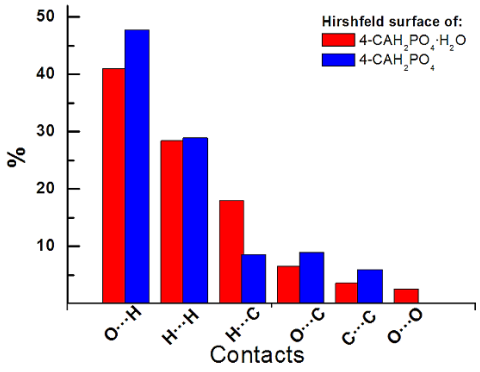

Figure 11. Percentage contributions to the Hirshfeld surface area of various close intermolecular contacts for 4-CAH_2PO_4·H_2O (red) and 4-CAH_2PO_4(blue) [8].

The relative strengths in the interaction energies in the individual directions of 4-CAH_2PO_4·H_2O are represented by cylinder-shaped energy frameworks (Figure 12a-c). In 4-CAH_2PO_4·H_2O crystals, the intermolecular packing is mainly stabilized by the anion cation coulombic attraction, which is obvious from unusually high values of interaction energies ranging from -200 to -800 kJ/mol. This is evident from the predominant electrostatic contribution compared to the minor contribution of dispersion forces in the energy framework of the crystals (Figure 12). Although hydrogen-bonded organic framework structure, as demonstrated through the electrostatic framework, we can see a tight cohesive framework of dispersion interactions which also underpin the structure of both crystals. A similar type of 3D topology was observed in 4-carboxyanilinium phosphite, bis(4-carboxyanilinium) sulfate, bis(4-carboxyanilinium) selenate trihydrate, and bis(4-carboxyanilinium) selenate [36-38]. 3D topology plots of 4-CAH_2PO_4 (Reference [8] CCDC deposition number 647348) showing electrostatic (red), dispersion (green) and total energy (blue for binding, gold for non-binding) contributions are shown in Figure 12d-f. The columbic attraction energies range from -100 to -500 kJ/mol in 4-CAH_2PO_4.

3.6. DFT calculations

3.6.1 Geometrical optimization of 4-CAH_2PO_4·H_2O

The geometric parameters of 4-CAH_2PO_4·H_2O structure were optimized using the DFT / B3LYP level with the 6-31G basis set. The optimized molecular structure of 4-CAH_2PO_4·H_2O with atom labeling scheme is shown in Figure 13a. The plot showing the correlation between the experimental and theoretical values of the bond distances obtained is shown in Figure 13b. When the experimental and theoretical values of bond length are compared, it is found that the theoretical bond lengths are slightly longer than those obtained from XRD data. The small discrepancies seen in the bond parameters are due to the fact that the theoretical calculations are carried out on an isolated molecule and the XRD data are obtained for the bulk molecules where the packing effects and intermolecular interactions play an important role in keeping the molecules together. The optimized C-C bond lengths of the phenyl ring were in the range of 1.3936 to 1.405 Å, which seems to be reliable and is in agreement with the experimental values obtained of the C-C bond lengths in the phenyl ring.

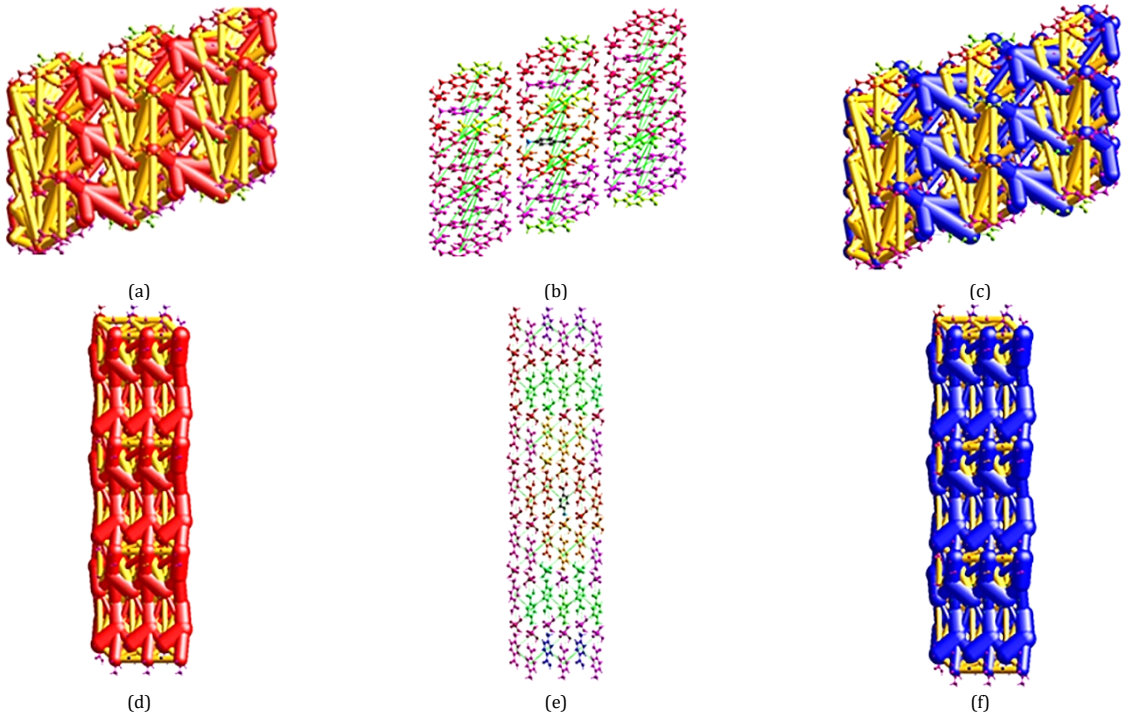

Figure 12. Energy framework diagrams for a 3×3×3 supercell of 4-$CAH_2PO_4{\cdot}H_2O$ (a, b, c) and 4-CAH_2PO_4 (d, e, f) (Reference [8] CCDC Deposition Number 647348) crystal structures viewed along the crystallographic *a* axis. The cylindrical radius is proportional to the relative strength of the corresponding energy and was adjusted to a scale factor of 45 kJ/mol with a cut-off value of 5 kJ/mol for all energies. The electrostatic (a, d), dispersion (b, e), and total energy (c, f) terms are colored red, green, and blue, respectively.

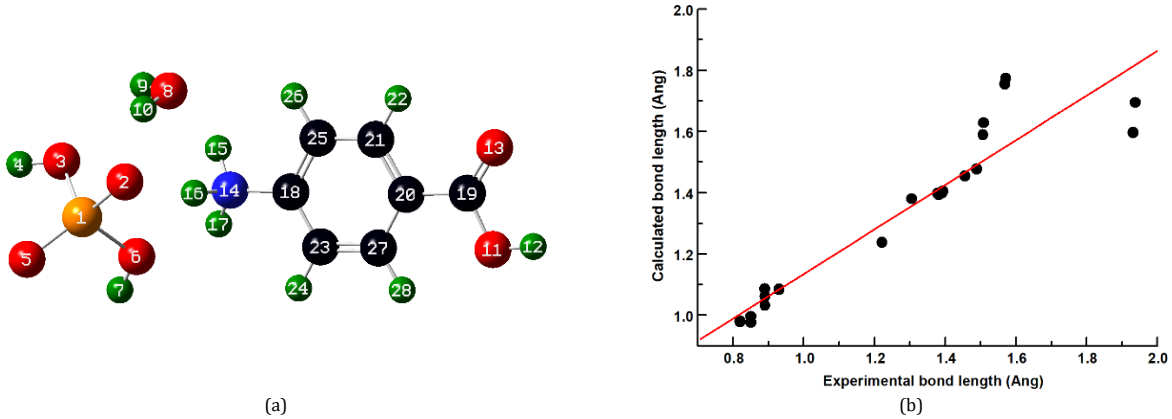

Figure 13. (a) The theoretically optimized molecular structure of 4-carboxyanilinium dihydrogen phosphate monohydrate with labeled atoms and (b) Plot depicting the graphical correlation between the experimental and theoretical values of the bond distances obtained by DFT/B3LYP level with 6-31G basis sets.

The optimized P-O bond lengths were 1.5889 to 1.6284 Å for P=O bonds and 1.7554 to 1.7734 Å for P-O-H bonds, which seems to be reliable. The amine N-H···O hydrogen bond appears to be stronger in theoretical calculations due to the orientation of the phosphate anion and water molecule. The experimental and calculated values of the hydrogen bond in (i) N-H···O=P were 1.9312 Å (exp) and 1.5966 Å (opt), respectively, and (ii) N-H···O-H (water) were 1.9374 Å (exp) and 1.6947 Å (opt), respectively. From the theoretical values, it is observed that the most optimized bond lengths and bond angles are slightly larger than the experimental value, because the theoretical calculations were carried out on molecules in the gaseous phase, while the experimental results correspond to molecules in solid crystalline states [39,40].

The theoretical calculation and analysis of the frontier orbitals, HOMO (highest occupied molecular orbital) and LUMO (lowest unoccupied molecular orbital) of a molecule help to understand and determine its chemical reactivity and kinetic stability. To understand the chemical reactivity and kinetic stability of 4-$CAH_2PO_4.H_2O$, the 3D plots of its HOMO and LUMO orbitals were obtained. The calculated energy gap, ΔE of 4-$CAH_2PO_4.H_2O$ is 5.1114 eV (Figure 14). A molecule with a large HOMO-LUMO gap will be a hard molecule. However, if the molecule has a small HOMO-LUMO gap, it will be a soft molecule. The ionization energy can be correlated with the chemical reactivity of atoms and molecules. The higher the ionization energy, the higher the stability and chemical inertness and vice versa. The ionization energy (I) and the electron affinity (A) can be expressed through the orbital energies of HOMO and LUMO as I = - E_{HOMO} = 7.2665 eV and A = - E_{LUMO} = 2.1551eV. Using the value of I and A, various properties of the 4-$CAH_2PO_4.H_2O$ complex have been calculated and are reported in Table 6.

Table 6. Theoretically calculated I, A, ΔE, η, χ, μ, ω, S, and ΔN_{max} of 4-$CAH_2PO_4.H_2O$ using the orbital energies of HOMO and LUMO.

Ionization energy (I)	I = - E_{HOMO}	7.2665 eV
Electron affinity (A)	A = - E_{LUMO}	2.1551eV
Energy gap (ΔE)	$\Delta E = E_{LUMO}$-E_{HOMO}	5.1114 eV
Global hardness (η)	η = (I-A)/2	2.5557 eV
Electronegativity (χ)	$\chi = (I+A)/2$	4.7111 eV
Electronic chemical potential (μ)	μ = -(E_{HOMO}+E_{LUMO})/2	4.7108 eV
Global electrophilicity index (ω)	ω = -(μ^2/2η)	-4.3394 eV
Global softness (S)	S = (1/ η)	0.3913 eV^{-1}
Maximum amount of electronic charge that the electrophile system may accept (ΔN_{max})	ΔN_{max} = -μ/η	1.8432

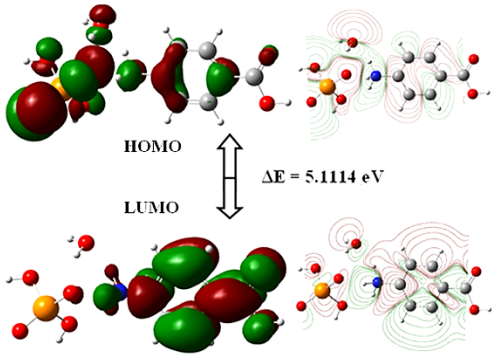

Figure 14. Calculated molecular orbital surfaces, its contour diagram, and the band gap of the HOMO and LUMO orbital in 4-$CAH_2PO_4.H_2O$ at the B3LYP/6-31G level.

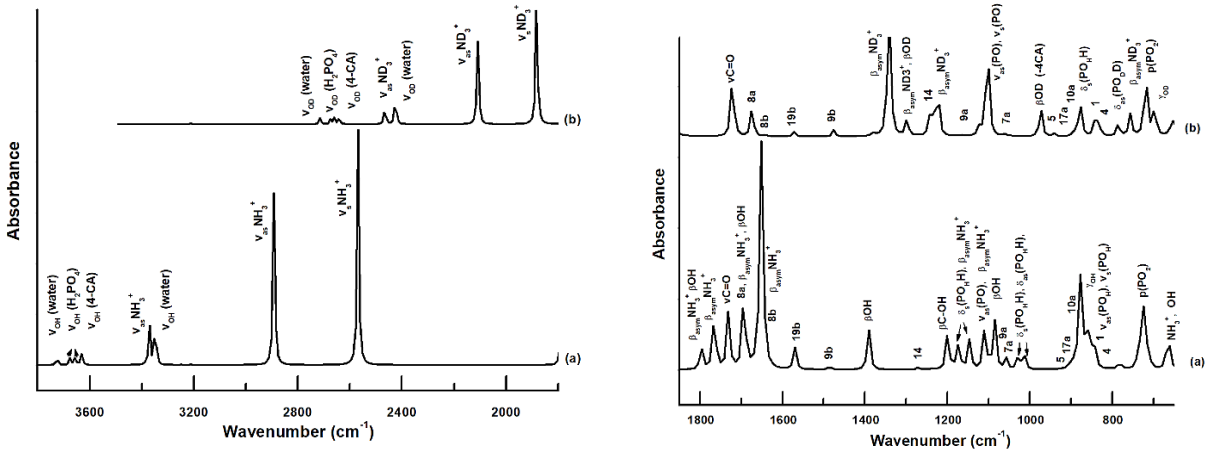

Figure 15. Theoretically calculated IR spectra of (a) 4-CAH_2PO_4·H_2O and (b) *d*4-CAH_2PO_4·H_2O in (A) 4000-1850 cm^{-1} and (B) 1850-650 cm^{-1}. The vibration mode assigned is done using Gaussian 09W.

3.6.2. Vibrational spectra of 4-CAH_2PO_4·H_2O

The vibrational spectra of 4-CAH_2PO_4·H_2O and *d*4-CAH_2PO_4·H_2O (the deuterated functional group) were obtained using the Gaussian 09 program with DFT/B3LYP level and 6-31G basis set. The assignment of different vibration modes seen in the calculated IR spectra of 4-CAH_2PO_4·H_2O is given in Table 5. The experimentally and theoretically obtained spectra were quite similar but with a shift in the frequency value. However, the experimentally obtained spectra were broad as the measurement was done on the bulk sample, and the calculated IR was obtained assuming that the molecule was isolated and in the gas phase. Figures 15a and 15b show the theoretically calculated IR spectra of 4-CAH_2PO_4·H_2O and *d*4-CAH_2PO_4·H_2O with the vibration mode assigned using Gaussian 09W. The 4-CAH_2PO_4·H_2O molecule has five functional groups: a para-substituted benzene ring, $-NH_3^+$, -COOH, -OH (water), and $H_2PO_4^-$. The functional groups in *d*4-CAH_2PO_4·H_2O were deuterated, $-ND_3^+$, -COOD, -OD (water), and -POD. In the 4000-1850 cm^{-1} region, the prominent stretching modes of the functional groups $-NH_3^+$, -COOH, -OH, and $H_2PO_4^-$ are seen that get shifted to a higher frequency on deuteration (Figure 15A). Similar behavior is seen in the 1850-650 cm^{-1} region, where in the deuterated counterpart the frequency is shifted to a higher value. The vibration modes of the C=O and P=O and the benzene ring are hardly affected by deuteration. Thus, a very good correlation could be seen between the experimentally and theoretically obtained spectra of 4-CAH_2PO_4·H_2O.

3.7. Non-covalent interaction (NCI) and Quantum theory of atom in molecule (QTAIM) analysis

3.7.1. Non-covalent interaction analysis

The noncovalent interaction (NCI), also known as reduced density gradient (RDG), is a methodology to identify and visualize weak interactions such as van der Waals, hydrogen bonds, and steric clashes within molecules [41]. The RDG for the molecules can be calculated using the electron density and its first derivative, as given in Equation 1. Thus, the RDG(r) function is a dimensionless form of the electron density gradient norm function, used to describe the deviation from the

homogeneous electron distribution. For regions far from the molecule, the electron density decays exponentially to zero; hence, the reduced gradient will have very large positive values. However, in the region of covalent bonding and noncovalent interactions, the reduced gradient has very small values. Therefore, to study the noncovalent interactions in a molecular system, the plot of the reduced gradients, RDG(r) versus ρ(r) is plotted and examined in the low reduced gradient regions (*i.e.* for the region where ρ(r) is small).

$$RDG(r) = \frac{1}{2(3\pi^2)^{\frac{1}{3}}} \frac{|\nabla\rho(r)|}{\rho(r)^{\frac{4}{3}}} \quad (1)$$

The second largest eigenvalue of the Hessian matrix of electron density, λ_2 and ρ can be used to distinguish these noncovalent interactions. For which a real space function, the sign(λ_2)ρ is defined and when this sign(λ_2)ρ (a.u.) function is plotted against RDG(r), a few spikes are observed. On the basis of the sign(λ_2) and ρ values, the following regions are defined. Strong attraction (halogen bond and hydrogen bond) if: (ρ > 0 and λ_2 < 0) blue. Van der Waals interaction if: (ρ ≈ 0 and λ_2 ≈ 0, *i.e.* very near to 0) green color (>-0.02 to < 0.005) region indicated in Figure 16a. Strong repulsion (Steric effect in the ring and cage) if (ρ > 0 and λ_2> 0) red.

The sign(λ_2)ρ function can also be represented using different colors based on its value, as mentioned above. The spikes obtained by plotting the sign(λ_2)ρ (a.u.) function against RDG(r) are classified into three types, the blue spike region, the green spike region, and the red spike region. By mapping the cross-section area of the spikes at a particular value of RDG(r), the RDG isosurface can be constructed. From this pictorial representation of RDG isosurfaces, both the location of the weak interaction and the type of interactions present in the molecule can be easily identified.

The noncovalent interactions present in 4-$CAH_2PO_4 \cdot H_2O$ complex were investigated using the Multiwfn 3.7 [24] and the graph obtained is shown in Figure 16a. From Figure 16a, it is evident that 4-$CAH_2PO_4 \cdot H_2O$ has steric, van der Waals and hydrogen bond interactions. There are spikes seen at very negative region of sign(λ_2)ρ, indicating that the 4-$CAH_2PO_4 \cdot H_2O$ compound contains an attractive intermolecular interaction. There are also spikes in the positive region indicating the presence of a steric effect in 4-$CAH_2PO_4 \cdot H_2O$. In Figure 16a, six spikes are seen, with their peak at position as per CP positions in AIM theory. The spikes around 0.020 and 0.010 a.u. represent the steric hindrance. The spikes around -0.010 a.u. represent the van der Waals force of attraction. The spikes seen around -0.035 and -0.05 a.u. are pertaining to hydrogen bond formation. The spike seen around -0.025 a.u. could be due to strong van der Waals force of attraction, weak hydrogen bond or both. These different interactions seen in 4-$CAH_2PO_4 \cdot H_2O$ can be represented pictorially by generating RDG isosurfaces using two cube files generated by Multiwfn 3.7 and viewed in the VMD 1.9.3 tool [24,42]. The structure of 4-$CAH_2PO_4 \cdot H_2O$ complex showing different isosurfaces of RDG is shown in Figure 16b. The red isosurfaces seen in the middle of the aromatic rings represent the presence of steric hindrance within the aromatic ring. The red and green isosurfaces seen near the -COOH region indicate the presence of both steric hindrance and van der Waals attraction in this region. In the cation: anion: water interface region, red, green, and blue-colored isosurfaces are seen, indicating the presence of steric hindrance, van der Waals attraction, and hydrogen bond interaction. The hydrogen bonds N-H···O (between NH_3^+ and water), and O···H-O (between $H_2PO_4^-$and water) are strong, as indicated by the presence of blue isosurfaces of RDG. While the N-H···O (between NH_3^+ and $H_2PO_4^-$) hydrogen bond interaction is relatively weak.

3.7.2 Quantum theory of atom in molecule (QTAIM) analysis

Bader's topology analysis technique is used to find the electron density in 'atoms in molecules' (AIM) theory, which is also known as 'the quantum theory of atoms in molecules' (QTAIM) [43]. In topology analysis, the points where the gradient norm of the function value is zero (except at infinity) are called as critical points (CPs). The CPs are classified into four types, nuclear critical point (NCP) (3, -3), bond critical point (BCP) (3, -1), ring critical point (RCP) (3, +1) and cage critical point (CCP) (3, +3) according to how many eigenvalues of the Hessian matrix of real space function are negative. QTAIM has both geometrical and topological features of electron density and its derivatives. The bond critical points (BCPs) of curvature (3, -1) mark the topological saddle points along 'bond lines' of maximum density between the nuclei. Thus, QTAIM is a useful tool for characterizing the topological properties of chemical bonds. The presence of chemical bonds between atoms and interatomic interactions is revealed by the presence of bond critical points (BCPs). The QTAIM method provides information on the electron density of a system that governs the properties at BCPs. The QTAIM theory gives information on variations of electron density due to the formation of bonds or complexes [43].

The QTAIM data of 4-$CAH_2PO_4 \cdot H_2O$ complex was generated using Multiwfn 3.7 and viewed with the VMD 1.9.3 tool. In the pictorial plot of the 4-$CAH_2PO_4 \cdot H_2O$ complex generated, the nonbonded interactions are represented by the bond critical points of curvature (3, -1) as shown in Figure 17. From Table 7 and Figure 17, it is observed that there are four BCPs between nonbonded atoms (a) N-H···O, (b) N-H···O, (c) O-H···O, and (d) N-H···O and four ring critical points (RCPs). The charge density (ρ), Laplacian of charge density ($\nabla^2\rho$), ellipticity (ε), energy density H(r), and hydrogen bond interaction energy (E_{HB}) calculated for these four BCPs obtained from QTAIM analysis are given in Table 7. The values of ρ(r) and $\nabla^2\rho$ at BCPs were in the range 0.0253 to 0.0627 a.u. and 0.0421 to 0.1429 a.u., respectively (Table 7) and therefore satisfy the Koch and Popelier criterion [44]. Bond ellipticity (ϵ) at different BCPs is defined as ε =((λ_1/λ_2)-1), where λ_1 and λ_2 are eigen values of Hessian of the electron density at BCP. This quantity estimates the extent to which the electron density is deformed in one direction relative to another. Thus, bond ellipticity is a measure of anisotropy of the curvature of the electron density (ρ(r)) in the direction normal to bond [43,45]. Therefore, ellipticity provides a measure of π or σ character of the chemical bonds. Hence, the ellipticity factor reflects the stability of the bonds [45]. A high value of ellipticity (ε > 0.1) indicates a π character of the bond, while a lower value reflects an σ character of the bond. In the 4-$CAH_2PO_4.H_2O$ complex, the value of the four BCPs was in the range 0.0295 to 0.0963 indicate these interactions to have σ character (Table 7). The interaction energies at the BCPs are calculated using the Equation (2 and 3) proposed by Emamian *et al.* [46].

$$BE_{(kcal/mole)} = -332.34 \times \rho(r_{BCP})_{(a.u)} - 1.0661 \quad (2)$$

(for charged complex) with a mean absolute percentage error (MAPE) of 10%

$$BE_{(kcal/mole)} = -223.08 \times \rho(r_{BCP})_{(a.u)} + 0.7423 \quad (3)$$

(for neutral complex) with a mean absolute percentage error (MAPE) of 14.7%

4-$CAH_2PO_4 \cdot H_2O$ is a charged complex. The calculated interaction energies (kcal/mol) for BCP at a, b, c, and d were -9.48739, -21.92024, -12.90466 and -17.95912, respectively (Table 7). Thus, the interaction energy for BCP at b > d > c > a. Therefore, the strongest non-bonded interaction (hydrogen bond) in the 4-$CAH_2PO_4.H_2O$ complex was for the BCP at N-H···O (b) having the value of -21.9202 kcal/mol.

Table 7. Parameters obtained from QTAIM analysis: charge density (ρ(r)), Laplacian of charge density ($\nabla^2\rho$), ellipticity (ε), potential energy density V(r), energy density H(r) and calculated H-bond interaction energy (E_{HB}) for the BCPs of the 4-$CAH_2PO_4.H_2O$ complex.

BCP (Interacting groups)	Density of all electrons ρ(r) (a.u.)	Laplacian of charge density $\nabla^2\rho$ (a.u.)	Ellipticity of electron density, ε	Energy density H(r) (a.u)	E_{HB} (kcal/mol)
(a) N-H···O, (-NH_3^+···$H_2PO_4^-$)	0.02534	0.08930	0.029521	-0.0002	-9.48739
(b) N-H···O, (-NH_3^+···$H_2PO_4^-$)	0.06275	0.18648	0.061555	-0.0054	-21.92024
(c) O-H···O, (Water···$H_2PO_4^-$)	0.03562	0.11162	0.096310	-0.0023	-12.90466
(d) N-H···O, (-NH_3^+···Water)	0.05083	0.15592	0.040958	-0.0032	-17.95912

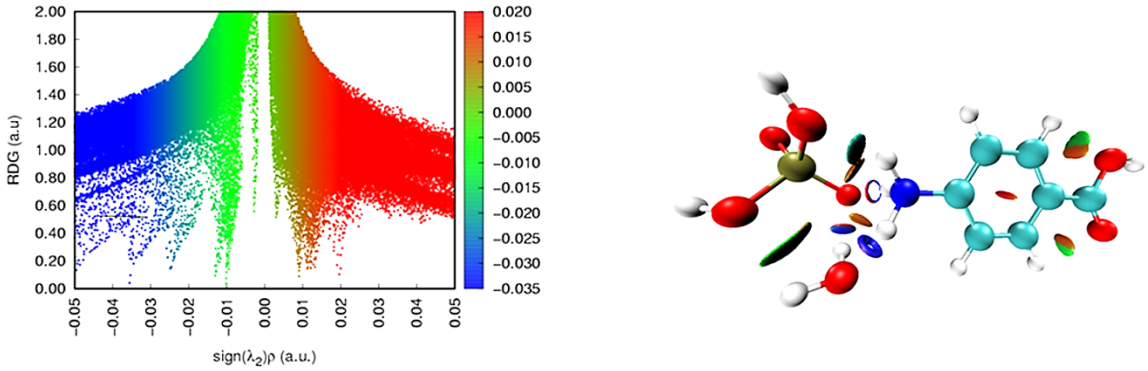

(a) (b)

Figure 16. The non-covalent interaction in 4-$CAH_2PO_4{\cdot}H_2O$ complex depicted by the presence of (a) spikes obtained by plotting the sign(λ_2)ρ (a.u.) function against RDG(r) and (b) RDG isosurfaces obtained by plotting NCL iso-surface at 0.5 iso-value (blue : H-bond, green: van der Waals attraction and red: steric hindrance).

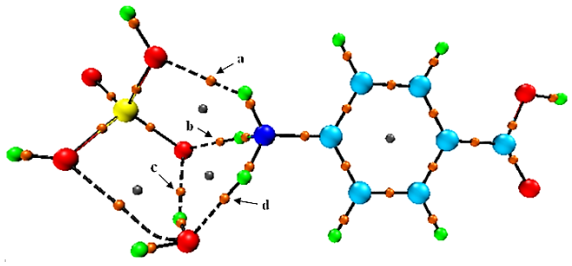

Figure 17. QTAIM molecular graph of the optimized 4-$CAH_2PO_4{\cdot}H_2O$ complex showing a graphical representation of bond critical points (small orange spheres), ring critical points (small gray sphere), and bond paths (black lines).

The total energy of hydrogen bond interaction involved in the formation of the stable 4-$CAH_2PO_4{\cdot}H_2O$ complex is -62.271 kcal/mol. According to Rozas *et al.* [47] the interactions at the different BCPs can be classified as follows: for strong hydrogen bonds ($\nabla^2\rho_{BCP} < 0$, $H_{BCP} < 0$), for medium hydrogen bonds ($\nabla^2\rho_{BCP} > 0$, $H_{BCP} < 0$) for weak hydrogen bonds ($\nabla^2\rho_{BCP} > 0$, $H_{BCP} > 0$). From Table 7, it is seen that for 4-$CAH_2PO_4{\cdot}H_2O$ complex all BCP fall in the medium hydrogen bonds category as $\nabla^2\rho_{BCP} > 0$, $H_{BCP} < 0$ in all 4 BCPs.

4. Conclusion

4-Carboxyanilinium dihydrogen phosphate monohydrate (4-$CAH_2PO_4{\cdot}H_2O$) was synthesized and investigated using FTIR spectroscopy, single-crystal XRD, differential, scanning calorimetry and computational analysis done using Gaussian 09W, CrystalExplorer 21, and Multiwfn 3.7 software. The crystal structure obtained belongs to the triclinic space group *P*-1, with two 4-carboxyanilinium cations, two dihydrogen phosphate ($H_2PO_4^-$) anions, and two water molecules in an asymmetric unit. The $H_2PO_4^-$ anion in the inorganic layer is linked and forms a long chain by hydrogen bond interaction between P-OH and -P=O groups of the adjacent $H_2PO_4^{-1}$ anions in the same layer. The phosphate layers are interconnected by the 4-CA cations of the organic layers by strong ionic and hydrogen-bond interactions. The interesting observation is that there is no hydrogen bond interaction between neighboring 4-carboxyanilinium cations within the organic layer. The 4-CA-cations are connected through a three-dimensional network of strong charge-assisted N-H···O and C-OH···O hydrogen bonds with $H_2PO_4^-$ and water molecules. Such an extensive three-dimensional hydrogen-bonding framework stabilizes the crystal structure. Most of the vibrational bands of 4-$CAH_2PO_4{\cdot}H_2O$ could be assigned based on the known IR assignments of the parent compounds (4-ABA, *d*4-ABA, and H_2PO_4) and also by comparing with the spectra of deuterated 4-$CAH_2PO_4{\cdot}H_2O$. The fingerprint plot of 4-$CAH_2PO_4{\cdot}H_2O$ obtained using Hirshfeld surface analysis indicated that the short O···H contacts were the most prominent interaction (41.1%) and this was followed by H···H (28.4%) and H···C (18%) contacts. The 3D topology of the strong charge-assisted hydrogen bonds in 4-$CAH_2PO_4.H_2O$ was obtained by plotting energy framework using CrystalExplorer 21. High values of interaction energies ranging from -200 to -800 kJ/mol were obtained. Quantum chemical calculations were performed in the gas phase using DFT with a hybrid function B3LYP at 6-31G basis set. The calculated IR spectra of the DFT optimized 4-$CAH_2PO_4{\cdot}H_2O$ complex were similar to its experimentally obtained spectra. NCI analysis indicated that the 4-$CAH_2PO_4.H_2O$ complex has steric, van der Waals, and hydrogen bond interactions. The hydrogen bonds N-H···O (between NH_3^+ and water), and O···H-O (between $H_2PO_4^-$ and water) were strong as indicated by the presence of blue RDG iso-surfaces. From the QTAIM analysis of 4-$CAH_2PO_4{\cdot}H_2O$ complex, four intermolecular hydrogen bonds were located. The hydrogen bond: N-H···O(-NH_3^+···$H_2PO_4^-$) > N-H···O(-NH_3^+···Water) > O-H···O(Water···$H_2PO_4^-$) > N-H···O(-

$NH_3^+\cdots H_2PO_4^-$) energies were calculated to be -21.92024, -17.95912 -12.90466 and -9.48739 kcal/mol, respectively, and which according to Rozas *et al.* [47] fall in the medium hydrogen bonds category. Thus, the thermal, vibrational, and computational results corroborate well with the structural data of 4-$CAH_2PO_4{\cdot}H_2O$ complex. 4-$CAH_2PO_4{\cdot}H_2O$ complex structure and its computational analysis are also compared with that of 4-carboxyanilinium dihydrogen phosphate (4-CAH_2PO_4).

Acknowledgements

The authors thank the Heavy Water Board, Bhabha Atomic Research Center, Trombay, Mumbai 400085, India, for supply of D_2O (99.4% isotopic purity).

Supporting information

CCDC-2288228 contains the supplementary crystallographic data for this article (4-carboxyanilinium dihydrogen phosphate monohydrate (4-$CAH_2PO_4{\cdot}H_2O$)). These data can be obtained free of charge via www.ccdc.cam.ac.uk/data_request/cif, or by emailing data_request@ccdc.cam.ac.uk, or by contacting The Cambridge Crystallographic Data Center, 12 Union Road, Cambridge CB2 1EZ, UK; fax: +44(0)1223-336033.

Disclosure statement

Conflict of interest: The author declares that they have no conflict of interest.
Ethical approval: All ethical guidelines have been followed.
Sample availability: Samples of the compound are available from the author.

Funding

Research work is carried out at the Bhabha Atomic Research Center, Trombay, Mumbai 400085, India, which is funded by the Indian government.

ORCID and Email

Lata Panicker
lata_panicker@yahoo.com
lata@barc.gov.in
https://orcid.org/0000-0001-5448-7502

References

[1]. Wojtaś, M.; Ga¸gor, A.; Czupiński, O.; Pietraszko, A.; Jakubas, R. 2,4,6-Trimethylpyridinium perchlorate: Polar properties and correlations with molecular structure of organic–inorganic hybrid crystal. *J. Solid State Chem.* **2009**, *182*, 3021–3030.
[2]. Parola, S.; Julián-López, B.; Carlos, L. D.; Sanchez, C. Optical properties of hybrid organic-inorganic materials and their applications. *Adv. Funct. Mater.* **2016**, *26*, 6506–6544.
[3]. Dos Santos, L.; Macchi, P. The role of hydrogen bond in designing molecular optical materials. *Crystals (Basel)* **2016**, *6*, 43–56.
[4]. Thakuria, R.; Delori, A.; Jones, W.; Lipert, M. P.; Roy, L.; Rodríguez-Hornedo, N. Pharmaceutical cocrystals and poorly soluble drugs. *Int. J. Pharm.* **2013**, *453*, 101–125.
[5]. Bharate, S. S. Recent developments in pharmaceutical salts: FDA approvals from 2015 to 2019. *Drug Discov. Today* **2021**, *26*, 384–398.
[6]. Mahé, N.; Nicolaï, B.; Allouchi, H.; Barrio, M.; Do, B.; Céolin, R.; Tamarit, J.-L.; Rietveld, I. B. Crystal structure and solid-state properties of 3,4-diaminopyridine dihydrogen phosphate and their comparison with other diaminopyridine salts. *Cryst. Growth Des.* **2013**, *13*, 708–715.
[7]. Benali-Cherif, N.; Abouimrane, A.; Sbai, K.; Merazig, H.; Cherouana, A.; Bendjeddou, L. *p*-Carboxyphenylammonium dihydrogenmono phosphate monohydrate. *Acta Crystallogr. Sect. E Struct. Rep. Online* **2002**, *58*, o160–o161.
[8]. Benali-Cherif, N.; Direm, A.; Allouche, F.; Soudani, K. Hydrogen bonding in 4-carboxyanilinium dihydrogenphosphate. *Acta Crystallogr. Sect. E Struct. Rep. Online* **2007**, *63*, o2272–o2274.
[9]. Agilent (2015). CrysAlis PRO. Agilent Technologies Ltd, Yarnton, Oxfordshire, England.
[10]. Sheldrick, G. M. *SHELXT*– Integrated space-group and crystal-structure determination. *Acta Crystallogr. A Found. Adv.* **2015**, *71*, 3–8.
[11]. Sheldrick, G. M. Crystal structure refinement with *SHELXL*. *Acta Crystallogr. C Struct. Chem.* **2015**, *71*, 3–8.
[12]. Dolomanov, O. V.; Bourhis, L. J.; Gildea, R. J.; Howard, J. A. K.; Puschmann, H. *OLEX2*: a complete structure solution, refinement and analysis program. *J. Appl. Crystallogr.* **2009**, *42*, 339–341.
[13]. Spackman, P. R.; Turner, M. J.; McKinnon, J. J.; Wolff, S. K.; Grimwood, D. J.; Jayatilaka, D.; Spackman, M. A. *CrystalExplorer*: a program for Hirshfeld surface analysis, visualization and quantitative analysis of molecular crystals. *J. Appl. Crystallogr.* **2021**, *54*, 1006–1011.
[14]. Turner, M. J.; Mckinnon, J. J.; Wolff, S. K.; Grimwood, D. J.; Spackman, P. R.; Jayatilaka, D.; Spackman, M. A. (2017) CrystalExplorer 21, University of Western Australia, Perth, Australia.
[15]. McKinnon, J. J.; Spackman, M. A.; Mitchell, A. S. Novel tools for visualizing and exploring intermolecular interactions in molecular crystals. *Acta Crystallogr. B* **2004**, *60*, 627–668.
[16]. Spackman, M. A.; Jayatilaka, D. Hirshfeld surface analysis. *CrystEngComm* **2009**, *11*, 19–32.
[17]. Spackman, M. A.; McKinnon, J. J. Fingerprinting intermolecular interactions in molecular crystals. *CrystEngComm* **2002**, *4*, 378–392.
[18]. Turner, M. J.; Grabowsky, S.; Jayatilaka, D.; Spackman, M. A. Accurate and efficient model energies for exploring intermolecular interactions in molecular crystals. *J. Phys. Chem. Lett.* **2014**, *5*, 4249–4255.
[19]. Mackenzie, C. F.; Spackman, P. R.; Jayatilaka, D.; Spackman, M. A. *CrystalExplorer*model energies and energy frameworks: extension to metal coordination compounds, organic salts, solvates and open-shell systems. *IUCrJ* **2017**, *4*, 575–587.
[20]. Frisch, M. J.; Trucks, G. W.; Schlegel, H. B.; Scuseria, G. E.; Robb, M. A.; Cheeseman, J. R.; Montgomery, J. A.; Vreven, T.; Kudin, K. N.; Burant, J. C.; Millam, J. M.; Iyengar, S. S.; Tomasi, J.; Barone, V.; Mennucci, B.; Cossi, M.; Scalmani, G.; Rega, N.; Petersson, G. A.; Nakatsuji, H.; Hada, M.; Ehara, M.; Toyota, K.; Fukuda, R.; Hasegawa, J.; Ishida, M.; Nakajima, T.; Honda, Y.; Kitao, O.; Nakai, H.; Klene, M.; Li, X.; Knox, J. E.; Hratchian, H. P.; Cross, J. B.; Adamo, C.; Jaramillo, J.; Gomperts, R.; Stratmann, R. E.; Yazyev, O.; Austin, A. J.; Cammi, R.; Pomelli, C.; Ochterski, J. W.; Ayala, P. Y.; Morokuma, K.; Voth, G. A.; Salvador, P.; Dannenberg, J. J.; Zakrzewski, V. G.; Dapprich, S.; Daniels, A. D.; Strain, M. C.; Farkas, O.; Malick, D. K.; Rabuck, A. D.; Raghavachari, K; Foresman, J. B.; Ortiz, J. V.; Cui, Q.; Baboul, A. G.; Clifford, S.; Cioslowski, J.; Stefanov, B. B.; Liu, G.; Liashenko, A.; Piskorz, P.; Komaromi, I.; Martin, R. L.; Fox, D. J.; Keith, T.; Al-Laham, M. A.; Peng, C. Y.; Nanayakkara, A.; Challacombe, M.; Gill, P. M. W.; Johnson, B.; Chen, W.; Wong, M. W.; Gonzalez, C.; Pople, J. A. Gaussian 09, Revision A.02, Gaussian, Inc., Wallingford CT, 2009.
[21]. Dennington, R.; Keith, T. A.; Millam, J. M. GaussView, Version 6, Semichem Inc.; Shawnee Mission, KS, 2016.
[22]. Becke, A. D. A new mixing of Hartree–Fock and local density-functional theories. *J. Chem. Phys.* **1993**, *98*, 1372–1377.
[23]. Becke, A. D. Density-functional exchange-energy approximation with correct asymptotic behavior. *Phys. Rev. A Gen. Phys.* **1988**, *38*, 3098–3100.
[24]. Lu, T.; Chen, F. Multiwfn: A multifunctional wavefunction analyzer. *J. Comput. Chem.* **2012**, *33*, 580–592.
[25]. Johnson, C. K. (1976). ORTEPII. Report ORNL-5138. Oak Ridge National Laboratory, Tennessee, USA.
[26]. Panicker, L.; Thomas, S. P.; Wadawale, A.; Girija, K. G.; Row, T. N. G. Reversible order-disorder phase transition and interaction topology in 4-carboxyanilinium nitrate. *J. Mol. Struct.* **2021**, *1227*, 129542.
[27]. Benali-Cherif, N.; Direm, A.; Allouche, F.; Boukli-H-Benmenni, L.; Soudani, K. 4-Carboxyanilinium hydrogensulfate. *Acta Crystallogr. Sect. E Struct. Rep. Online* **2007**, *63*, o2054–o2056.
[28]. Świsłocka, R.; Samsonowicz, M.; Regulska, E.; Lewandowski, W. Molecular structure of 4-aminobenzoic acid salts with alkali metals. *J. Mol. Struct.* **2006**, *792–793*, 227–238.
[29]. Samsonowicz, M.; Hrynaszkiewicz, T.; Świsłocka, R.; Regulska, E.; Lewandowski, W. Experimental and theoretical IR, Raman, NMR spectra of 2-, 3- and 4-aminobenzoic acids. *J. Mol. Struct.* **2005**, *744–747*, 345–352.
[30]. Versányi, G. Assignments for Vibrational Spectra of 700 Benzene Derivatives, Akademiai Kiado, Budapest, Hungary, 1973.
[31]. Nakamoto, K. *Infrared and Raman spectra of inorganic and coordination compounds: Part A: Theory and applications in inorganic chemistry*; Wiley: Hoboken, NJ, USA, 2008.
[32]. Oubouaza, R.; Benson, M.; Wojciechowski, J.; Chtita, S.; Tridane, M.; Belaaouad, S. Synthesis, crystal structure, vibrational study and DFT computation of barium dihydrogenomonophosphate Ba(H2PO4)2. *Biointerface Res. Appl. Chem.* **2021**, *12*, 1120–1133.
[33]. Robertson, W. H.; Johnson, M. A. Molecular aspects of Halide ion hydration: The cluster approach. *Annu. Rev. Phys. Chem.* **2003**, *54*, 173–213.
[34]. Klähn, M.; Mathias, G.; Kötting, C.; Nonella, M.; Schlitter, J.; Gerwert, K.; Tavan, P. IR spectra of phosphate ions in aqueous solution: Predictions of a DFT/MM approach compared with observations. *J. Phys. Chem. A* **2004**, *108*, 6186–6194.
[35]. Baril, J.; Max, J.-J.; Chapados, C. Titrage infrarouge de l'acide phosphorique. *Can. J. Chem.* **2000**, *78*, 490–507.
[36]. Panicker, L. 4-Carboxyanilinium phosphite: A structural, vibrational, thermal and computational study. *J. Mol. Struct.* **2023**, *1288*, 135773.
[37]. Panicker, L. Structural, vibrational and thermal study of Bis(4-Carboxyanilinium) sulphate a new organo-sulphate adduct of 4-amino benzoic acid. *J. Mol. Struct.* **2022**, *1267*, 133631.

[38]. Panicker, L. Structural, vibrational, thermal and computational studies of new organo-selenate compounds bis(4-carboxyanilinium) selenate and bis(4-carboxyanilinium) selenate trihydrate. *J. Mol. Struct.* **2024**, *1296*, 136764.
[39]. Tamer, Ö.; Sefa Atalay, A.; Avci, D.; Atalay, Y.; Tarcan, E.; Marchewka, M. K. Optimized geometry, vibration (IR and Raman) spectra and nonlinear optical activity of p-nitroanilinium perchlorate molecule: A theoretical study. *Mater. Sci.-Pol.* **2016**, *34*, 192–203.
[40]. Mohankumar, V.; Karunagaran, N.; Pandian, M. S.; Ramasamy, P. Density functional theory calculations and Hirshfeld surface analysis of propyl-para-hydroxybenzoate (PHB) for optoelectronic application. *Mater. Sci.-Pol.* **2020**, *38*, 386–393.
[41]. Johnson, E. R.; Keinan, S.; Mori-Sánchez, P.; Contreras-García, J.; Cohen, A. J.; Yang, W. Revealing noncovalent interactions. *J. Am. Chem. Soc.* **2010**, *132*, 6498–6506.
[42]. Humphrey, W.; Dalke, A.; Schulten, K. VMD: Visual molecular dynamics. *J. Mol. Graph.* **1996**, *14*, 33–38.
[43]. Bader, R. F. W. *Atoms in Molecules: A Quantum Theory*; Clarendon Press: Oxford, England, 1994.
[44]. Koch, U.; Popelier, P. L. A. Characterization of C-H-O hydrogen bonds on the basis of the charge density. *J. Phys. Chem.* **1995**, *99*, 9747–9754.
[45]. Yang, Y.-Z.; Liu, X.-F.; Zhang, R.-B.; Pang, S.-P. Joint experimental and theoretical studies of the surprising stability of the aryl pentazole upon noncovalent binding to β-cyclodextrin. *Phys. Chem. Chem. Phys.* **2017**, *19*, 31236–31244.
[46]. Emamian, S.; Lu, T.; Kruse, H.; Emamian, H. Exploring nature and predicting strength of hydrogen bonds: A correlation analysis between atoms-in-molecules descriptors, binding energies, and energy components of symmetry-adapted perturbation theory. *J. Comput. Chem.* **2019**, *40*, 2868–2881.
[47]. Rozas, I.; Alkorta, I.; Elguero, J. Behavior of ylides containing N, O, and C atoms as hydrogen bond acceptors. *J. Am. Chem. Soc.* **2000**, *122*, 11154–11161.